eology and origin
Basin, Arizona:

eongsang andesite
lustries Engineers

ns in the Yakuōji
Soc. Tokyo Jour.,

ated with hydro-
CON. GEOL., v. 59,

opper Creek area,

ivity in the middle
Geol. Soc. Korea

The geology and
ia-pipe, San Fran-
ina: ECON. GEOL.,

nineralized breccia

n, an unrecognized
ON. GEOL., v. 64, p.

ages of the major
apan: ECON. GEOL.,

71, Geologic, min-
ating to the origin
pipes, Chile: ECON.

k, A. H., 1968, A
supergene mineral
Chile: Inst. Mining
166–B169.
ondyke Quadrangle,
U. S. Geol. Survey

e geology and min-
oc. Korea Jour., v.

Economic Geology
Vol. 72, 1977, pp. 769 795

Petrogenesis of the Copper-Bearing Skarn at the Mason Valley Mine, Yerington District, Nevada

MARCO T. EINAUDI

Abstract

Skarn formation at the Mason Valley mine occurred at a depth of 2,000 m on the outer fringe of a contact metasomatic aureole related to a Jurassic granodiorite to quartz monzonite batholith. The skarn is located in Upper Triassic limestone at the contact with a stratigraphically lower tuff unit and is systematically zoned relative to this contact. The general zonal sequence toward marble is: garnet, garnet-pyroxene-sulfides, pyroxene-sulfides, tremolite-magnetite-calcite, talc-magnetite-calcite, and dolomite-calcite. The zones migrated outward with time.

Electron microprobe data indicate that garnets and pyroxenes in the barren garnet footwall zone have compositions similar to the districtwide early metasomatic hornfelses and are represented by low-iron diopsides and intermediate grandites. Pure andradite, as overgrowths and in cross-cutting veins, becomes more abundant as the hanging-wall skarn is approached. Both garnets and pyroxenes shift abruptly to higher iron contents in the hanging-wall skarn which formed at the contact between the early garnet zone and dolomitized limestone. Garnets maintain a constant lower limit of 55 mole percent andradite and are zoned to pure andradite. Later garnets, contemporaneous with chalcopyrite deposition, consist of pure andradite. The iron content of pyroxene increases gradually and systematically toward the marble contact, from an average value of 36 mole percent hedenbergite in the inner garnet-pyroxene zone to 56 mole percent hedenbergite in pyroxene vein centers on the marble contact, and then drops abruptly to 15 mole percent hedenbergite in vein envelopes. Two generations of amphibole are represented by: (1) early tremolite (0 to 10 mole percent ferrotremolite) associated with magnetite-calcite in outermost vein envelopes in marble; and (2) actinolite which contains the same Fe/Mg ratio as associated pyroxene and is contemporaneous with chalcopyrite deposition in the pyroxene and garnet-pyroxene zones.

The initial silication process, as represented by zoned veins at the marble contact, may be attributed to isothermal metasomatic diffusion of Ca, Mg, and Si, with X_{CO_2} decreasing toward the vein centers. The abrupt appearance of new minerals coincides with the attainment of appropriate chemical potential values through metasomatism, rather than the crossing of isobaric univariant T-X_{CO_2} equilibria. Bulk composition gradients are extreme and are reflected in the rapid increase in iron content of tremolite and diopside over a few centimeters from vein envelope to vein center.

Within the main skarn zone, which formed at higher temperature and/or lower X_{CO_2}, bulk composition gradients are less extreme, and phase-composition trends are opposite to those that would be predicted by a simple isothermal diffusion model. The gradual inward decrease in the iron content of salite within skarn zones of relatively constant bulk composition may have been controlled in part by continuous Fe-Mg reactions.

Comparison with phase-composition data from similar zoned skarns indicates that variation of phase compositions within zones is a characteristic phenomenon, but that zonal composition trends in some cases are opposite to those established here.

Introduction

THERE is a singular lack of investigations aimed specifically at quantifying the zoning, paragenesis, and compositions of silicates associated with copper-bearing skarns. The present paper supplies data and discussion bearing on this problem with emphasis on field relations and chemical composition of coexisting garnet, pyroxene, and amphibole.

The Mason Valley mine (MVM) is ideally suited for study of these aspects of skarn geology because its zonal and paragenetic features are relatively unambiguous and simple. The skarn is well exposed and formed within a small volume of chemically homogeneous host rock during a single hydrothermal episode, much as a zoned alteration envelope on a vein.

The MVM is located in the Yerington district, Lyon County, Nevada, 2.5 km west of Mason. It is a small copper-bearing skarn deposit formed by metasomatic replacement of Triassic limestone on the outer fringe of a contact aureole related to the Yerington batholith of Jurassic age. The MVM yielded an estimated 1.5 million tons of 2.5 to 3.0 percent copper ore in the years 1912 to 1935. It was developed principally by two adits, the 300 and 400, to a depth of 175 m below the outcrop. Numerous underground workings expose the skarn zone.

The surface in the vicinity of the MVM was mapped on the scale 1 in. = 400 ft. The 300 and 400 mine levels were mapped on the scale 1 in. = 40 ft. Normal mapping procedures for rock types, faults, and mineralization were used, and detailed visual estimates were made of percent garnet, pyroxene, calcite, chalcopyrite, and pyrite. Particular attention was paid to textures and cross-cutting vein relations. Channel samples were taken after mapping was completed and were used to determine the bulk chemical and modal composition of the various mineral zones. Mineral relations were studied in 50 thin sections, and numerous samples were studied by X-ray diffraction. The composition of garnets, pyroxenes, and amphiboles from selected assemblages in nine polished thin sections were determined by electron microprobe analysis.

District Setting

The Yerington district is located 80 km east of the Sierra Nevada batholith in the western Great Basin province within a belt of Jurassic intrusives. One of these intrusives, the Yerington batholith, occupies much of the northern end of the Singatse Range. Strongly folded and faulted volcanic and sedimentary rocks form an east-west-trending septum 8 km long and up to 3 km wide between the Yerington batholith and a southern batholith. These rocks are metamorphosed and locally metasomatized and are part of a thick sequence of lower Mesozoic eugeosynclinal rocks forming a broad belt through western Nevada. A total thickness of about 3,000 m is exposed in the Singatse Range.

Sedimentary and intrusive rocks

The lower one-half of the lower Mesozoic section is composed of metamorphosed andesite and rhyolite flows, breccias, and sediments. A Rb-Sr isochron age of about 215 m.y., probably Middle Triassic, has been obtained from these rocks (Proffett, Livingston, and Einaudi, in prep.). The upper portion of the section is Late Triassic and Early to Middle(?) Jurassic. Mappable units 50 to 250 m thick consist of massive limestones, thin-bedded black calcareous shales, silicic volcanic sediments and flows, gypsum, and quartzite. Limestone beds constitute the host rock for numerous small copper-bearing skarns located on the outer fringe of a contact metasomatic aureole extending 600 to 1,800 m from the Yerington batholith.

The Yerington batholith is formed from an intrusive sequence initiated by the emplacement of a major volume of granodiorite, followed by moderate amounts of quartz monzonite, and terminated by the formation of porphyry copper deposits associated with quartz monzonite porphyry dike swarms within its central portion. Pyritic quartz monzonite porphyry dikes occur throughout the batholith in varying density, but only a few are found south of the main contact within the septum of Triassic sedimentary and volcanic rocks.

Contact aureole

A detailed description and discussion of contact metamorphism and metasomatism of Triassic rocks in the Yerington district will be presented elsewhere. Only a brief discussion is given here to set the context for the MVM skarn. The distribution of metasomatic rocks and the zoning of mineral assemblages indicate that the Yerington batholith, rather than the southern batholith, is responsible for these effects. Metasomatism occurred in two episodes, as first documented by Knopf (1918). An early stage produced garnet-pyroxene hornfelses near the batholith contact and recrystallization to hornblende hornfels facies rocks farther out. Garnets in the metasomatic hornfelses belong to the grossularite-andradite series and range from 24 to 68 mole percent andradite. The pyroxenes belong to the diopside-hedenbergite series and range in composition from 0 to 15 mole percent hedenbergite.

Brecciation of these early hornfelses was followed by formation of more iron rich garnets without pyroxene, locally accompanied by pink clinozoisite near the intrusive, and by the formation of andradite-salite skarns on the fringe of the metasomatic aureole in dolomitized marbles. Six skarn deposits are located in the Triassic septum west of Mason. Two of these, the Douglas Hill and Bluestone deposits, are located relatively close to the intrusive contact within the zone of early garnet-pyroxene hornfelses. Both are characterized by: (1) relatively low total sulfides, generally less than 5 volume percent; (2) relatively high chalcopyrite/pyrite ratios, generally greater than 10; (3) absence of magnetite or hematite; (4) a gangue dominated by andradite, with minor epidote at the Bluestone mine; (5) strong brecciation.

In a fringe position relative to the andradite-chalcopyrite skarns are the remaining four producers: Mason Valley, Western Nevada, Casting Copper, and McConnell mines, listed in order of decreasing production. All four formed in dolomitized marble on the fringe of the early hornfelses, 1,000 to 2,000 m from the batholith contact. These fringe skarns are characterized by: (1) relatively high total sulfides, in the range 10 to 25 volume percent; (2) very low chalcopyrite/pyrite ratios, generally lower than 1; (3) presence of trace quantities of magnetite on the marble contact; (4) a gangue dominated by coarse, bladed salite and andradite; (5) little or no evidence of brecciation.

wed by moderate
terminated by the
posits associated
ke swarms within
: monzonite por-
batholith in vary-
und south of the
of Triassic sedi-

ussion of contact
of Triassic rocks
sented elsewhere.
re to set the con-
tribution of meta-
neral assemblages
h, rather than the
for these effects.
odes, as first docu-
ly stage produced
he batholith con-
rnblende hornfels
n the metasomatic
te-andradite series
ent andradite. The
edenbergite series
o 15 mole percent

elses was followed
arnets without py-
k clinozoisite near
ion of andradite-
etasomatic aureole
deposits are located
on. Two of these,
eposits, are located
contact within the
nfelses. Both are
low total sulfides,
ent; (2) relatively
generally greater
or hematite; (4)
, with minor epi-
strong brecciation.
the andradite-chal-
g four producers:
, Casting Copper,
rder of decreasing
dolomitized marble
ses, 1,000 to 2,000
hese fringe skarns
ely high total sul-
ume percent; (2)
s, generally lower
ntities of magnetite
gue dominated by
e; (5) little or no

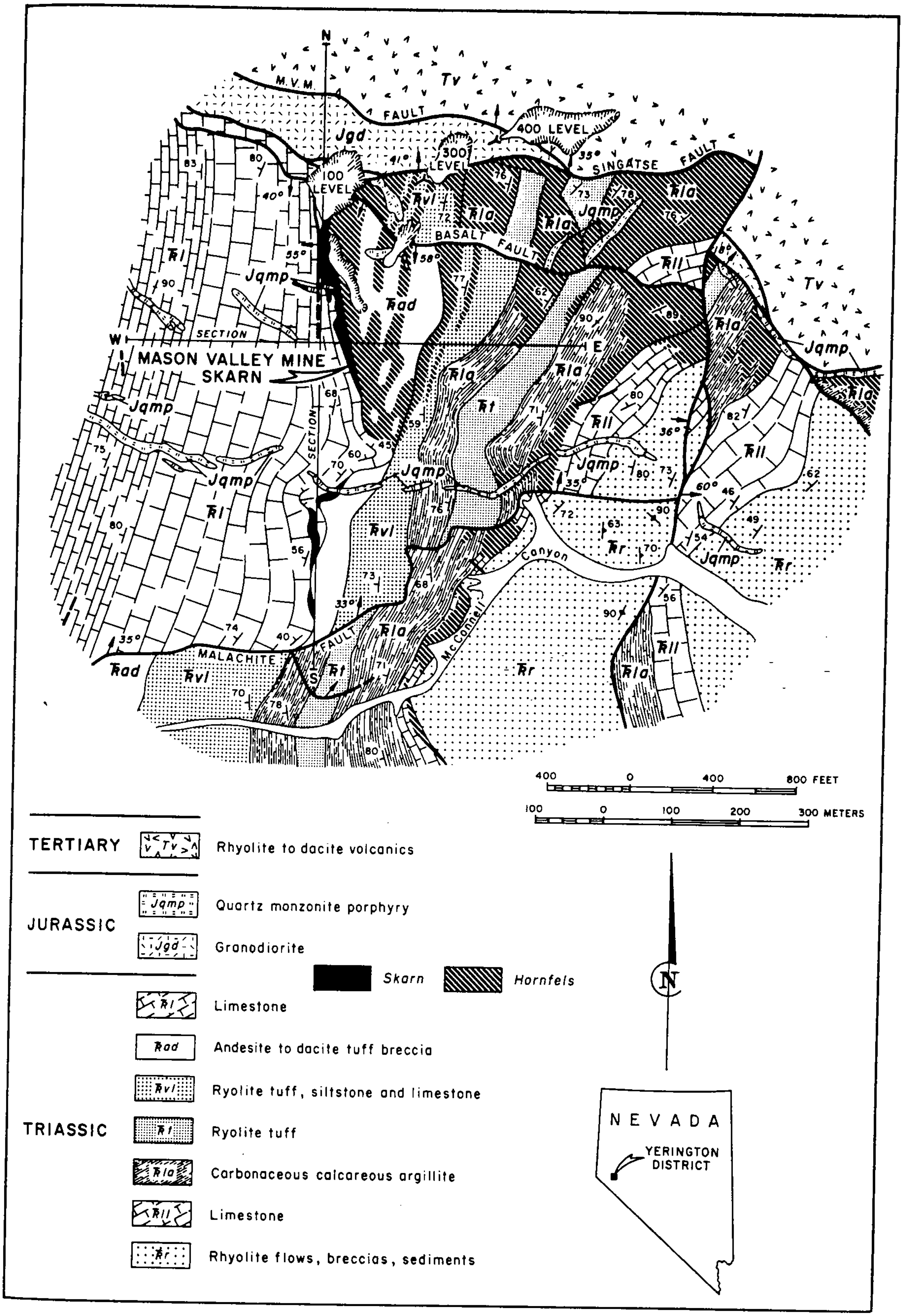

FIG. 1. Surface geologic map of the vicinity of the Mason Valley mine. Irregularity of flat fault traces is due to topography. Insert shows location of Yerington district in western Nevada.

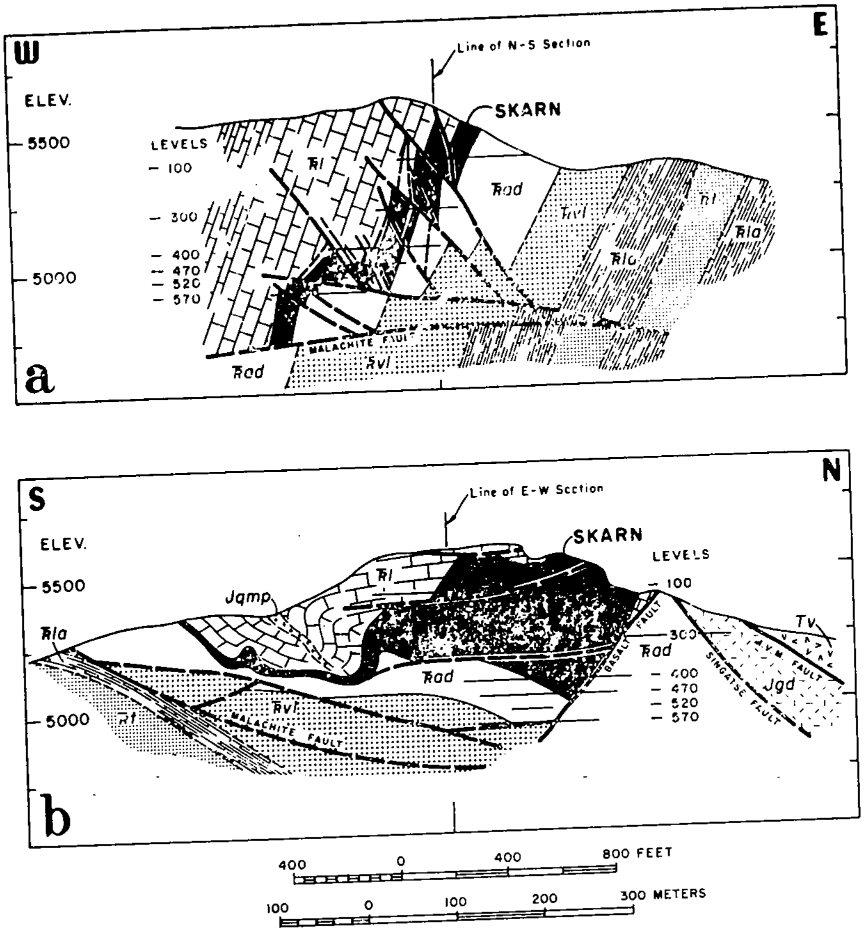

FIG. 2. a. East-west cross section, looking north, drawn at right angle to the strike of bedding and skarn. East-dipping faults are shown as cut by the flat Malachite fault, a relation suggested by the lack of offsets of the surface trace of the latter.

b. North-south cross section, looking west, drawn parallel to the strike of bedding and skarn. The Basalt and Malachite faults may join at depth to form a single spoon-shaped fault. Locations of cross sections are shown in Figure 1.

Cenozoic structure and depth of formation

Subsequent to the emplacement of the Jurassic batholiths and the formation of the contact aureole and its associated ore-bearing skarns, there ensued a long period of erosion during at least part of the Cretaceous and the early Tertiary. The resulting erosion surface was covered during late Oligocene to early Miocene time by a thick sequence of rhyolitic to dacitic ignimbrites and andesitic flows and breccias (Proffett and Proffett, 1976). Basin and range normal faulting commenced during the final phases of this volcanic activity in Miocene time. Faulting, accompanied by westward tilting, occurred on east-ward-dipping, concave upward, normal faults. An average tilt of at least 70° west has been documented for the Tertiary ignimbrites. All Mesozoic rocks are likewise tilted at least 70° to the west (Proffett, 1969, 1972).

The present surface, therefore, consists of repeated, fault-controlled partial cross sections. The fault block containing the MVM does not include the lower Tertiary erosion surface. Although a direct measurement of depth below this surface is not possible, a structural reconstruction of the contact aureole indicates Jurassic configuration of the contact aureole indicates that the MVM was located 1,700 m below the lower Tertiary surface. This figure represents a minimum depth of formation.

The depth of erosion over the top of the MVM during Cretaceous and early Tertiary time is estimated at 500 m or greater. This figure represents the removal of a minimum of 500 m of volcanic rocks, which may be extrusive equivalents of the Yerington batholith and which are preserved below the lower Tertiary surface in the Buckskin range, 10 km northwest of the MVM (Proffett, 1969). Recent mapping

TABLE 1. Chemical and Modal Composition of Fresh and Altered Rocks, Mason Valley Mine

Sample no. Rock type	F-12 Marble	F-11 Dolomite	MVM-3 Pyx	MVM-2 Pyx-gar	MVM-4 Gar-pyx Ore	MVM-1 Garnet	MVM-5 Gar-epid	F-10 Tuff
SiO_2	0.87	1.84	37.90	31.35	29.61	35.83	39.06	48.10
TiO_2	0.00	0.00	0.05	0.00	0.00	0.04	0.61	1.24
Al_2O_3	1.91	3.41	2.38	2.97	2.80	4.50	14.16	29.08
Fe_2O_3 (tot Fe)	0.00	0.00	24.12	27.07	26.88	21.76	12.22	11.75
MgO	0.70	11.64	7.16	4.53	2.57	1.95	3.32	0.24
MnO	0.01	0.02	0.15	0.10	0.18	0.08	0.17	0.01
CaO	52.54	41.02	20.58	23.22	23.60	30.91	28.06	1.05
Na_2O	0.18	0.41	0.38	0.45	0.35	0.33	0.49	1.32
K_2O	0.07	0.11	0.00	0.00	0.00	0.00	0.11	1.98
Cu	NA	NA	0.05	0.15	2.25	0.24	0.02	NA
S	0.006	0.006	10.08	13.28	10.31	1.41	0.053	0.043
Dr	2.13	2.76	3.15	3.10	3.06	3.03	2.67	2.96
Dm	2.69	2.76	3.54	3.72	3.87	3.46	3.34	2.95
Calcite	94	44	3	6	5	8	5	2
Quartz	Tr	—	4	—	6	6	3	20
Dolomite	—	54	—	—	—	—	—	—
Pyroxene	—	—	55	50	10	5	15	Tr
Amphibole	Tr	—	7	8	5	6	8	—
Garnet	—	—	5	10	52	68	40	—
Plagioclase	—	—	—	—	—	3	—	Tr
Epidote	—	—	—	—	—	—	10	—
Andalusite	—	—	—	—	—	—	—	34
Chlorite	Tr	—	—	—	—	4	10	10
Muscovite	—	Tr	—	—	—	—	5	—
Biotite	—	—	—	—	—	—	—	25
Montmorillonite	—	—	6	2	2	—	4	—
Magnetite	—	—	Tr	—	—	—	—	8
Pyrite	—	—	20	25	15	2.5	Tr	—
Chalcopyrite	—	—	Tr	0.3	5	0.5	—	—

Oxides in weight percent, minerals in volume percent. Tr = trace. Dr = measured rock density; Dm = measured mineral density; NA = not analyzed. Major elements, except Na and Mg, were determined by X-ray fluorescence; Na, Mg, and Cu by atomic absorption; S by a LECO induction furnace technique. Mineral percentages based on combined estimates from thin sections, bulk X-ray diffraction, and computation from chemical analyses.

by D. A. Heatwole shows that these volcanic rocks rest upon early Mesozoic sedimentary rocks equivalent to those immediately below the lower Tertiary surface near the MVM. The depth of formation of the MVM is therefore on the order of 2,200 m, equivalent to 600 bars lithostatic pressure.

Skarn Geology and Petrology

Sedimentary rocks

Rocks exposed in the vicinity of the MVM consist largely of Upper Triassic limestones and volcaniclastic rocks, which are correlative with part of the Oreana Peak Formation of the southern Pine Nut Range (Noble, 1962). These sedimentary rocks have a northerly strike and dip steeply west. Basin and range normal faulting has resulted in a complex outcrop pattern (Fig. 1).

Two sedimentary units are important at the MVM: a dacitic to andesitic tuff unit and a stratigraphically higher, thick-bedded limestone unit.

Tuff unit: The tuff unit is 60 to 150 m thick. Its base consists of interbedded arkosic sandstone, and tuffaceous argillite, 0 to 15 m thick. Andesitic to dacitic tuffs overlie the quartz-bearing clastics. South of the Malachite fault, where the rocks have suffered little or no metasomatism, these are medium-bedded, dark-greenish to black, fine-grained hornfelses containing lithic fragments up to several centimeters in size. The fragments are flattened parallel to bedding and the tuffaceous groundmass consists of a metamorphic aggregate of quartz, muscovite, chlorite, and magnetite. Andalusite may also be present associated with quartz, biotite, and magnetite. A chemical and mineral analysis of the tuff breccia is presented in Table 1 (No. F-10).

Limestone unit: The massive limestone unit is 240 to 270 m thick. The top of the unit is marked by a gradation to thin-bedded shaly limestone. The bulk of the limestone unit consists of massive, medium- to coarse-grained, gray to white calcite marble with little evidence of bedding. The marble is composed of a mosaic of interlocking calcite grains; quartz is absent or is present only in trace quantities, and white tremolite or small flakes of pale chlorite are locally present. The chemical analysis presented in Table 1 (No. F-12) confirms the low quartz content and the absence of dolomite.

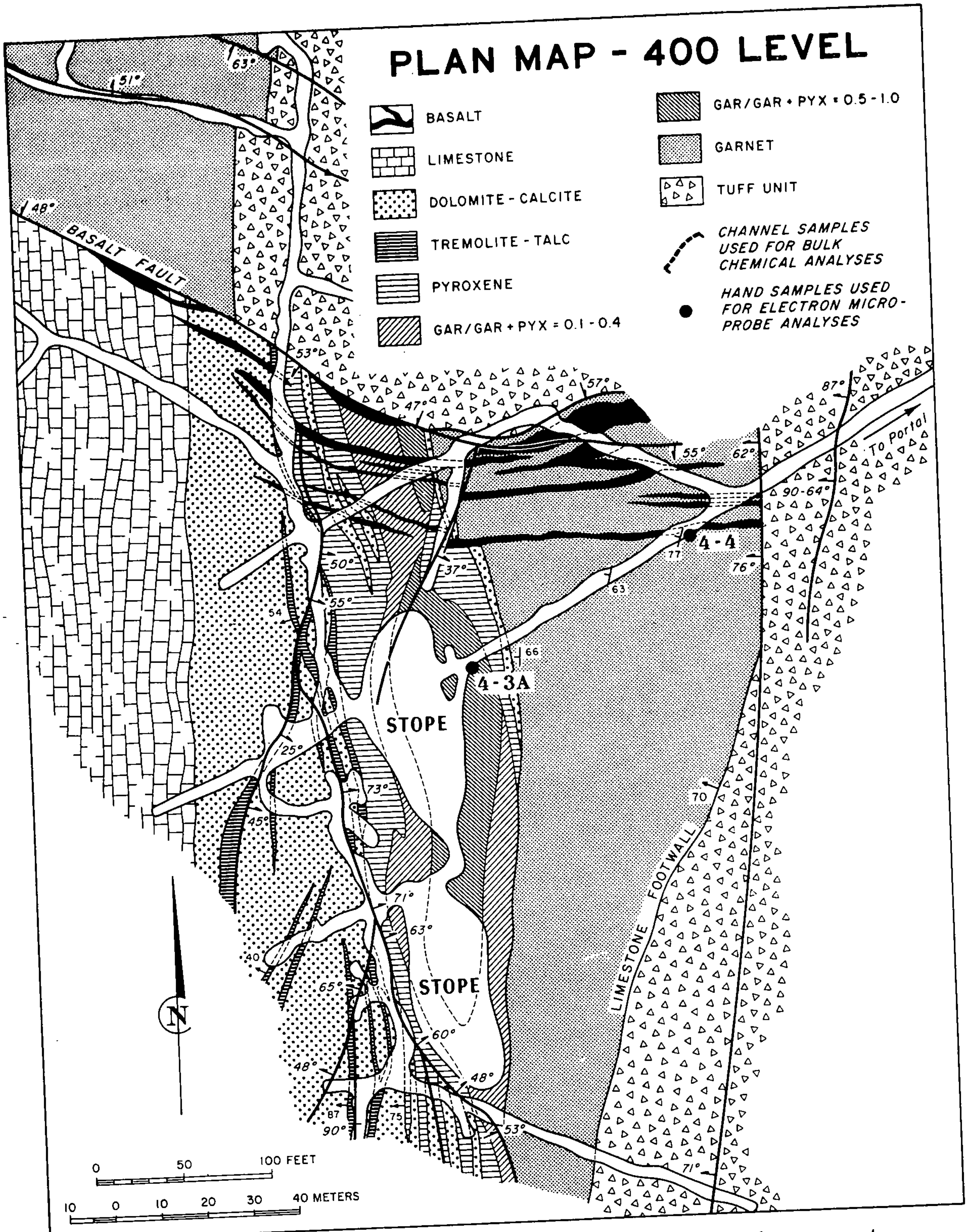

FIG. 3. Plan map of a portion of the 400 level, Mason Valley mine. Contacts between garnet-pyroxene zones are gradational, whereas contacts between pyroxene, tremolite, and marble are sharp.

Irregular patcl
weathering dolon
sive limestone un
tural control. Tl
probably of metas
The dolomite c
rarely exceeds 6(
chlorite, white m
quartz is absent.
of a bulk sample
outcrop is presen

Igneous rocks

Intrusive ignec
belong to the Y
The intrusive con
sic rocks is hidde
the MVM. Thi
blocks to the wes
struction suggests
900 m south of tl
The east-west s
the tilted fault blc
ment between fau
that its pretilt att
west striking. T
in detail and con
physes within a z
Granodiorite:
the MVM, in the
(Fig. 1). It is
by the Singatse fa
shaped, normal f
in an easterly
granodiorite pres
the MVM was ju
close to the lowe
and tilting. The
the north by the
shaped fault, the
The granodiori
granular, with 40
cent alkali feldspa
to 20 percent maf
lesser pyroxene a
4 percent magnet
trace of apatite
epidote replace p
this type of alter
minor pyrite.
Quartz monzo
monzonite porph
vicinity of the M
N 50°–80° W ar
The porphyry c
alkali feldspar, q

Irregular patches, several meters across, of buff-weathering dolomitic marble occur within the massive limestone unit and exhibit some degree of structural control. They often cross-cut bedding and are probably of metasomatic rather than diagenetic origin. The dolomite content is extremely variable and rarely exceeds 60 percent. Sparse amounts of talc, chlorite, white mica, and pyrite may be present, and quartz is absent. A chemical and mineral analysis of a bulk sample collected 60 m north of the MVM outcrop is presented in Table 1 (sample F-11).

Igneous rocks

Intrusive igneous rocks exposed near the MVM belong to the Yerington batholith of Jurassic age. The intrusive contact of the batholith with the Triassic rocks is hidden under the Singatse fault north of the MVM. This contact is exposed in other fault blocks to the west, however, and a structural reconstruction suggests that the MVM was situated about 900 m south of the main contact.

The east-west strike of the intrusive contact within the tilted fault blocks, and its general east-west alignment between fault blocks across the range, indicate that its pretilt attitude was nearly vertical, and east-west striking. The contact zone is highly irregular in detail and consists of abundant granodiorite apophyses within a zone averaging 300 m in width.

Granodiorite: Granodiorite is exposed north of the MVM, in the area of the 300 and 400 level adits (Fig. 1). It is separated from the Triassic rocks by the Singatse fault, which is an east-dipping, spoon-shaped, normal fault with 4,000 m of displacement in an easterly direction (Proffett, 1972). The granodiorite presently exposed in its hanging wall at the MVM was just northeast of the MVM and very close to the lower Tertiary surface before faulting and tilting. The granodiorite wedge is bounded on the north by the southern portion of another spoon-shaped fault, the MVM fault (Figs. 1 and 2).

The granodiorite is fine to medium grained, equigranular, with 40 to 50 percent plagioclase, 20 percent alkali feldspar, 10 to 15 percent quartz, and 10 to 20 percent mafic minerals, largely hornblende with lesser pyroxene and biotite. Accessories include 2 to 4 percent magnetite, 1 to 1.5 percent sphene, and a trace of apatite and zircon. Local chlorite and epidote replace plagioclase and mafic minerals, and this type of alteration is generally accompanied by minor pyrite.

Quartz monzonite porphyry: Dikes of quartz monzonite porphyry cut the Triassic rocks in the vicinity of the MVM (Figs. 1 and 2). They strike N 50°–80° W and dip moderately to the northeast. The porphyry contains phenocrysts of plagioclase, alkali feldspar, quartz, hornblende, and subordinate biotite set in a fine aplitic or aphanitic groundmass of quartz and alkali feldspar. They are similar in general appearance and mineralogy to the porphyry dikes which cut the granodiorite batholith and are undoubtedly of the same age. The porphyry dikes have negligible contact effects and appear to postdate skarn formation.

Zoning, morphology, and structure

The MVM skarn formed largely in limestone at the tuff contact (Figs. 1 and 2). The outcrop extends along this contact for 600 m, with an average width of 45 m in the northern one-half and 0 to 15 m in the south. It dips 70° west, parallel to bedding.

The skarn consists of two distinct elements of approximately equal widths (Figs. 3 to 5). The footwall, or eastern one-half, consists largely of garnet and contains 1 to 5 percent sulfides (Table 1, MVM-1). It is in contact on the east with epidote-grossularite skarn which formed in the tuff unit (Table 1, MVM-5). The hanging wall, or western one-half, consists dominantly of garnet and pyroxene and contains an average of 20 percent sulfides. The mineralogy and mineral compositions of the footwall skarn indicate that it belongs to the early stage of contact metasomatism. It is relatively uniform in composition throughout, and is referred to below as the garnet zone. The hanging-wall skarn is late relative to the footwall skarn. It formed in previously dolomitized limestone along the outer edge of the garnet zone.

Mineral zoning in the hanging-wall skarn is, as might be expected, very pronounced and systematic. The skarn may be treated as a large, zoned, alteration envelope with the center line located 0 to 15 m west of the western edge of the garnet zone (Fig. 5). Proceeding out from the center line to the dolomitic marble wall rock, the general zonal sequence is: (1) garnet-pyroxene, (2) pyroxene, and (3) marble contact zones. The marble contact zone contains pyroxene veins with zoned tremolite-talc-calcite envelopes. The central garnet-bearing zone pinches out along the center line to the south. The location of the footwall garnet zone relative to the hanging-wall skarn center line resulted in an asymmetric zonal development. The pyroxene and marble contact zones are best developed on the west.

The silicate zonal pattern and skarn morphology reveal that the dominant direction of flow of the metasomatic fluid was southward, away from the northern batholith contact, along a faulted and brecciated tuff-limestone contact during the early stage, and along bedding planes in marble during the formation of the hanging-wall skarn. The skarn fingers out along bedding to the south and consists of steeply west-dipping calc-silicate bands 2 to 10 m wide sepa-

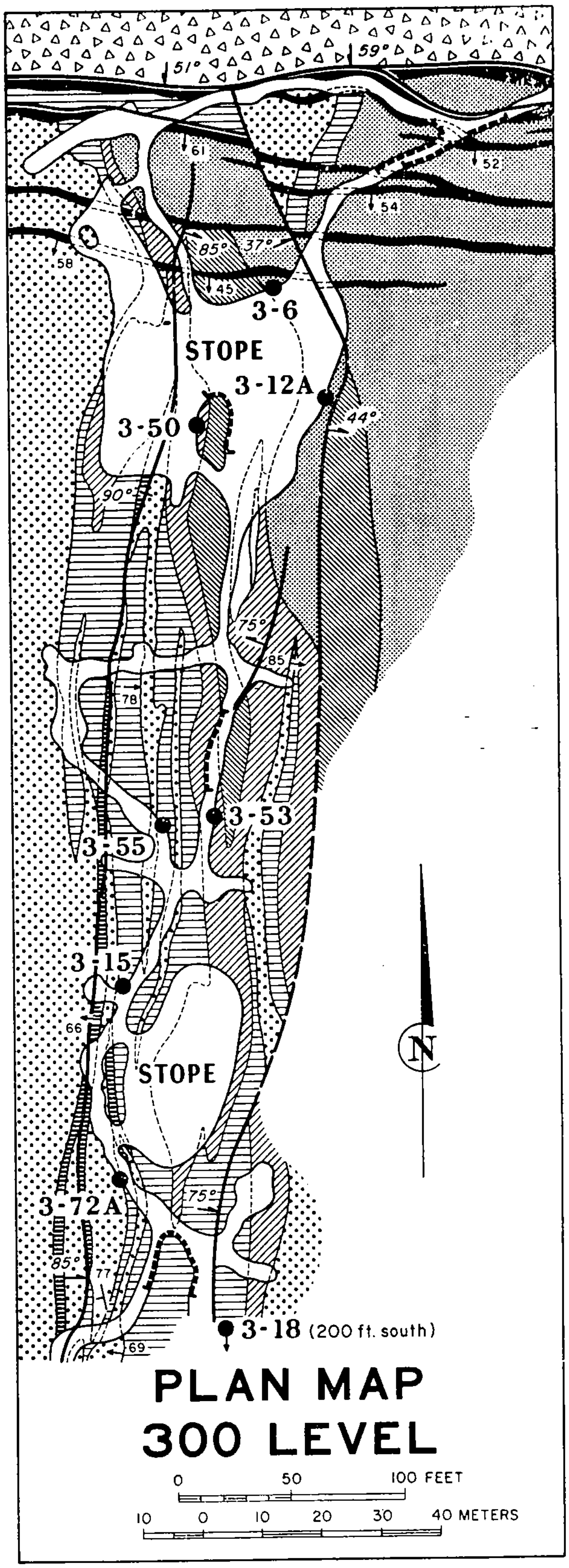

FIG. 4. Plan map of a portion of the 300 level, Mason Valley mine. Symbols are the same as in Figure 3.

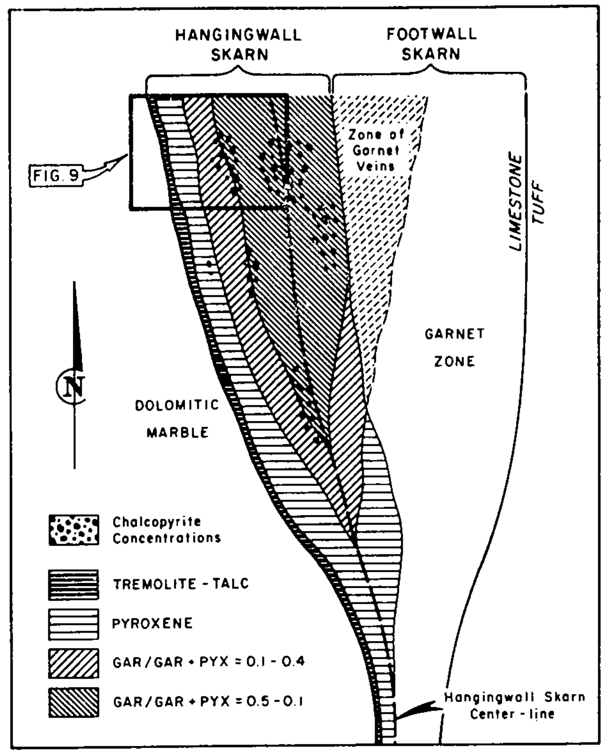

FIG. 5. Schematic map of mineral zoning and morphology. Length of skarn shown is approximately 150 m.

rated by marble. Movement of fluid at right angles to bedding was largely fracture controlled. Evidence of preskarn fractures exists only on the outer contact where silication is not pervasive and where calc-silicate veins up to several centimeters wide criss-cross the dolomitic marble. Continued fracturing during skarn formation is indicated by late silicate-sulfide assemblages cementing early assemblages within the hanging-wall skarn zone, and by veins of garnet cutting the footwall skarn.

Postskarn faulting had only a minor disruptive effect on the skarn zone. The oldest faults in the mine, which may be pre-Tertiary in age, strike north-south parallel to bedding, and dip 55° to 70° east. These faults have normal dip-slip displacements of 5 to 25 m, and offset ore zones and silicate zonal patterns. The youngest postskarn structure, which occurs near the north end of the skarn exposure, consists of a 50° south-dipping fault which offsets the skarn 75 m in a left-lateral sense. This fault zone was intruded by a swarm of basalt dikes, 0.5 to 1.5 m thick, which may have been feeders for the Pliocene basalt flows that cap the hills south of the MVM. Postdike movement is indicated by fault gouges along the dike contacts which contain southeast-plunging mullions. These mullions suggest that the last movement was in a direction compatible with an origin for the Basalt fault as the northern segment of an east-

TABLE 2. S
between colun
constituents.

CcTa(
TaCcM
Ta(Mt
Tr(Ccl
DiTrC
DiCcP
SaCcP

Abbreviatio

dipping, spoc
Locally, basa
against the sl
semblage can
the skarn dis
tse fault.

Paragenesis a

Though so
visible underg
vasive and re
ing becomes a
out the skarn
or veins hav
(2) higher ir
copyrite/pyrit
than the early
In both early
wall skarn, t
pyrite ratios d
The present s
zonal growth
having enable
Textures a
skarn zones
marble contac
9. The seque
is summarize
garnet, pyrox
Tables 3, 4, 5,
and amphibo
by electron m
tories, EMX)
chemically ho
as standards.
5.4 to 24.0 w
weight percen
percent. Back

TABLE 2. Sequence of Formation of Mineral Assemblages. Time increases downward in each column. Time comparisons between columns are tentative. Phases are listed in order of decreasing abundance and parentheses indicate minor or trace constituents.

Marble zone		Hanging-wall skarn Pyroxene zone	Garnet-pyroxene zone	Footwall skarn Garnet zone
				Cc(Ch)
				DoCc
				CcTr(ChTa)
				DiCc
				GrDiCc
				GrQzCc(Py)
				CcQzChEpPy
CcTa(Ch)				
TaCcMt(Ch)				
Ta(Mt)				
Tr(CcMt)				
DiTrCc(MtHm)	TrCcDo	DiCcPy(MtHm)	SaPy(Cc)	
DiCcPy(MtHm)		SaPyCc(MtHm)	GrSaPy(Cc)	
SaCcPy(MtHm)			AdPyCpCc	GrCcQzPy
		AcSaPyCpCc		AdCcPy(Cp)

Abbreviations as in Table 3, with addition of Ch = chlorite, Ep = epidote, Gr = grandite.

dipping, spoon-shaped, normal fault (Figs. 1 and 2). Locally, basalt dikes display sharp intrusive contacts against the skarn, but no influence on the skarn assemblage can be detected. North of the Basalt fault, the skarn disappears under the north-dipping Singatse fault.

Paragenesis and mineral compositions

Though some veining of skarn by later silicates is visible underground and in hand specimen, the pervasive and repetitive nature of fracturing and rehealing becomes apparent only in thin section. Throughout the skarn, the overgrowths, cementing materials, or veins have (1) higher garnet/pyroxene ratios, (2) higher iron content in garnet, (3) higher chalcopyrite/pyrite ratios, and (4) larger grain sizes than the early assemblages, fragments, or wall rock. In both early and late assemblages in the hanging-wall skarn, the garnet/pyroxene and chalcopyrite/pyrite ratios decrease to the south and toward marble. The present skarn pattern, therefore, is the result of zonal growth outwards, with continued fracturing having enabled solution flow.

Textures and mineral relations within the four skarn zones (garnet, garnet/pyroxene, pyroxene, marble contact) are illustrated in Figures 6, 8, and 9. The sequence of formation of mineral assemblages is summarized in Table 2, and the compositions of garnet, pyroxene, and amphibole are summarized in Tables 3, 4, 5, and 6 and Figure 7. Garnet, pyroxene, and amphibole were analyzed for Al, Fe, and Mg by electron microprobe (Applied Research Laboratories, EMX) using standard techniques. Three chemically homogeneous clinopyroxenes were used as standards. These range in total Fe as FeO from 5.4 to 24.0 weight percent, Al_2O_3 from 0.6 to 9.4 weight percent, and MgO from 0.7 to 19.9 weight percent. Background corrections were applied to all data. Drift corrections were obviated by the use of fixed beam current rather than fixed time to integrate intensities over an average time of 10 sec. No other corrections were applied to the data. Microprobe wavelength scans indicate that garnet, pyroxene, and amphibole are members of the grossularite-andradite, diopside-hedenbergite, and tremolite-ferrotremolite solid solution series, respectively. The composition of these phases will be referred to below in terms of mole percent of the iron end members: andradite (Ad), hedenbergite (Hd), and ferrotremolite (Ft).

Garnet zone: Overall, the zone contains 70 percent garnet, 10 percent pyroxene, and minor quartz, calcite, amphibole, plagioclase, chlorite, and pyrite (Table 1, MVM-1). Total sulfide abundance is in the range 2 to 4 percent, and the chalcopyrite/pyrite ratio averages 0.2. Faint relic bedding in the garnet zone is expressed by varying proportions of garnet and pyroxene and varying grain sizes. This zone consists predominantly of pale gray-green and buff,

TABLE 3. Some Common Skarn Minerals in the System Ca-Mg-Fe-Si-Cu-S_2-O_2-CO_2-H_2O. Minerals in parentheses do not occur at the MVM.

hematite	Hm	Fe_2O_3
magnetite	Mt	Fe_3O_4
pyrite	Py	FeS_2
chalcopyrite	Cp	$CuFeS_2$
calcite	Cc	$CaCO_3$
dolomite	Do	$CaMg(CO_3)_2$
quartz	Qz	SiO_2
(wollastonite)	Wo	$CaSiO_3$
(forsterite)	Fo	Mg_2SiO_4
talc	Ta	$Mg_3Si_4O_{10}(OH)_2$
tremolite	Tr	$Ca_2Mg_5Si_8O_{22}(OH)_2$
actinolite	Ac	$Ca_2(Mg, Fe)_5Si_8O_{22}(OH)_2$
(ferrotremolite)	Ft	$Ca_2Fe_5Si_8O_{22}(OH)_2$
diopside	Di	$CaMgSi_2O_6$
salite	Sa	$Ca(Mg, Fe)Si_2O_6$
(hedenbergite)	Hd	$CaFeSi_2O_6$
andradite	Ad	$Ca_3Fe_2Si_3O_{12}$

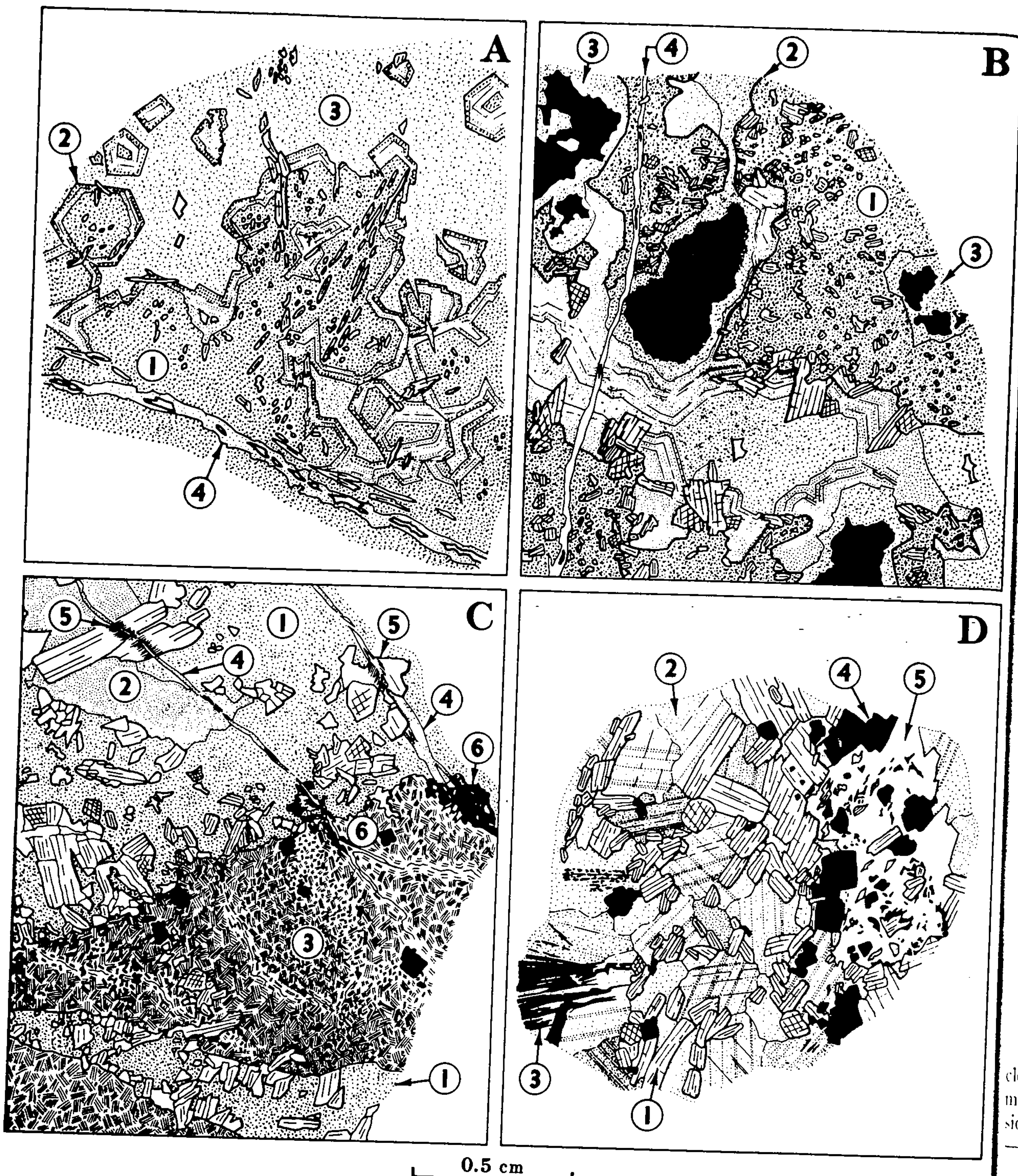

FIG. 6. Sketches of mineral relations in thin section.

A. Specimen 3–12A, footwall skarn. Early grandite-diopside assemblage (1) with grandite crystals zone from anisotropic cores (Ad_{35-50}) to isotropic, strongly banded rims (Ad_{70}) (2), overgrown by isotropic andradite (Ad_{100}) (3) plus calcite and cut by late grandite (Ad_{45-70}) vein (4) with final andradite-quartz-calcite filling.

B. Specimen 4-3A, hanging-wall skarn, garnet-pyroxene zone. Early fragments (1) of grandite (Ad_{50-60})-salite (Hd_{31-42}) cemented by isotropic andradite plus chalcopyrite (3). Fragment boundaries (2) are lined with coarse-grained salite crystals whose growth terminated

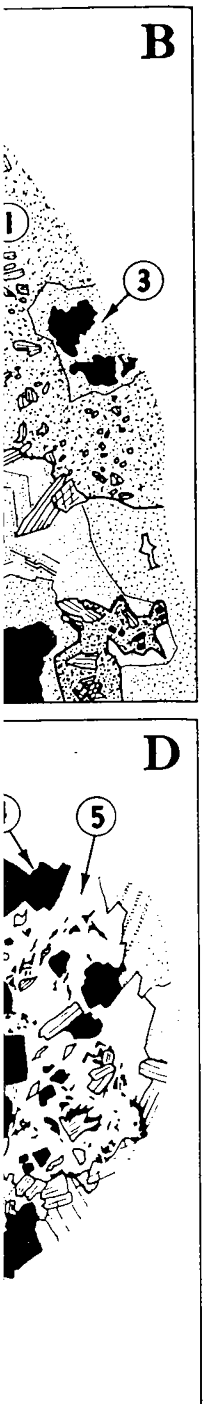

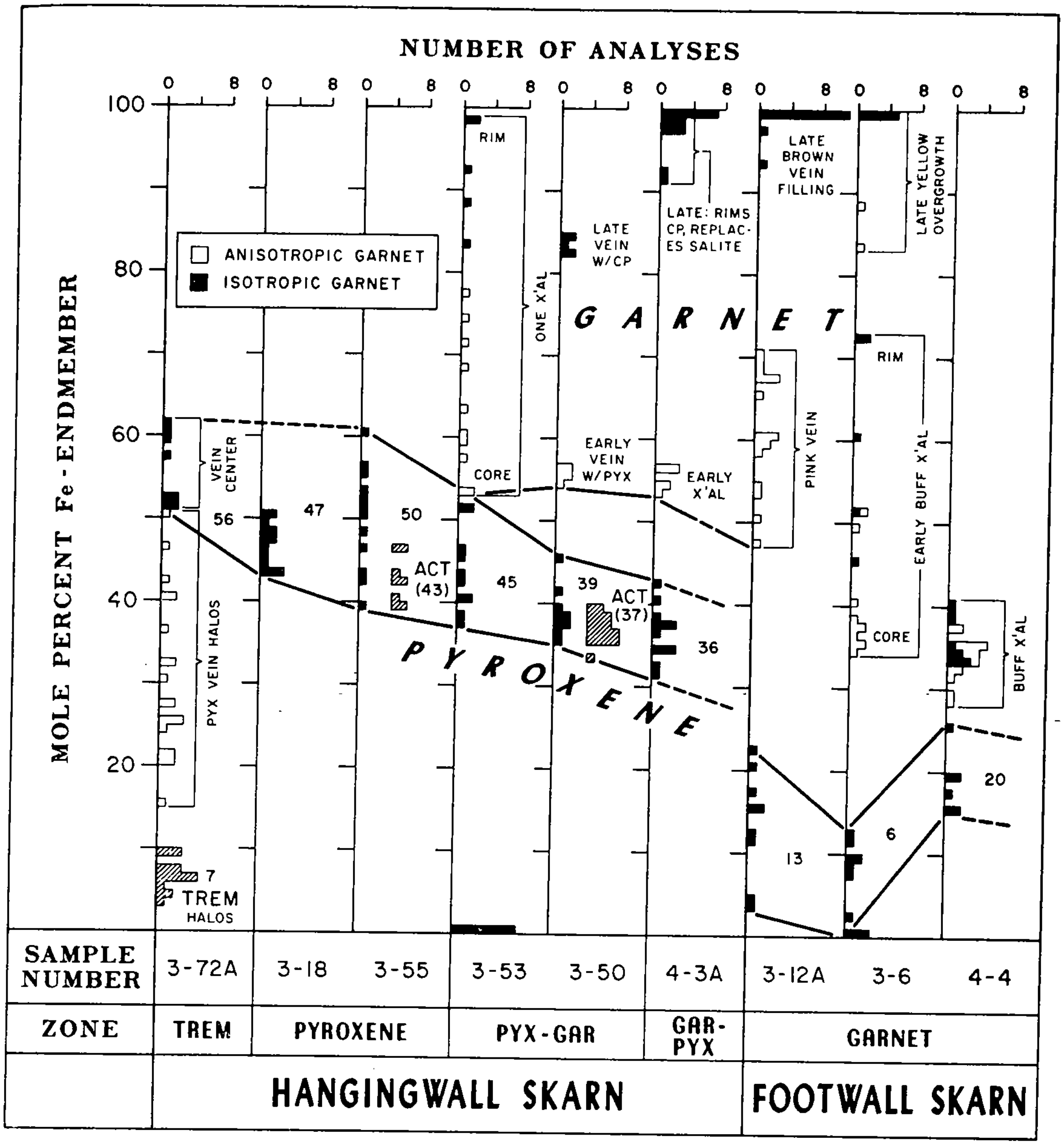

FIG. 7. Summary of electron microprobe analyses of garnet, pyroxene, and amphibole. Analyses are recalculated in terms of the iron end members andradite, hedenbergite, and ferrotremolite.

cloudy, largely anisotropic garnet crystals 0.2 to 1.0 mm in diameter which contain small ragged inclusions of pyroxene 0.02 to 0.5 mm in longest dimension. These inclusions are concentrated in the cores of the garnet crystals, suggesting that pyroxene was no longer forming during the final stages of garnet

at time of final Ad-Cp filling. Fragments and matrix are cut by andradite-chalcopyrite vein (4).

C. Specimen 3–50, hanging-wall skarn, outer portion of garnet-pyroxene zone. Grandite (Ad_{55})-salite (Hd_{35-45}) veins (1) with andradite (Ad_{95}) centers (2) cut fine-grained, clay-altered pyroxene skarn (3). Later andradite (Ad_{95}) veinlets with local chalcopyrite and calcite contain andradite envelopes in grandite (4) and actinolite envelopes in salite (5). At the point where the veinlets enter the pyroxene skarn (6) the vein filling changes to actinolite (Ft_{34-38}) and large patches of actinolite (Ft_{31-39})-chalcopyrite appear.

D. Specimen 3–15, hanging-wall skarn, pyroxene zone. Salite (1)-calcite (2)-magnetite (3)-pyrite (4) assemblage. Magnetite growth appears to have been controlled by calcite cleavage or pseudomorphs specular hematite. Actinolite (5) is intergrown with chalcopyrite and partially replaces salite.

TABLE 4. Partial Microprobe Analyses of Garnet (expressed as wt %)

Zone	Sample no.	Grain no.	No. anal.	Al_2O_3	tot Fe as Fe_2O_3	MgO	X_{Ad}	Range in X_{Ad}
G	4-4	2A	9	13.5	12.0	0.01	0.36	0.33–0.41
G	4-4	2B	9	13.9	11.2	0.01	0.34	0.29–0.37
G	4-4	2C	5	14.1	11.2	0.01	0.34	0.29–0.37
G	3-6	1A	15	11.0	15.0	0.02	0.46	0.34–0.73
G	3-6	1A core	9	12.9	12.4	0.01	0.38	0.34–0.45
G	3-6	1A rim	6	8.0	18.9	0.04	0.60	0.49–0.73
G	3-6	1B	7	0.8	29.6	0.00	0.96	0.84–1.0
G	3-12A	2A	6	0.02	30.5	0.05	0.96	0.99–1.0
G	3-12A	2B	5	0.00	30.9	0.00	1.0	none
G	3-12A	2C	17	7.9	19.5	0.00	0.61	0.48–0.70
G	3-12A	2D	5	0.43	30.4	0.00	0.98	0.94–1.0
G	3-12A	3B	6	0.00	31.0	0.01	1.0	none
G-P	4-3A	1A	6	9.0	17.6	0.00	0.55	0.54–0.57
G-P	4-3A	1B	6	0.16	30.4	0.01	0.99	none
G-P	4-3A	1C	5	0.23	30.3	0.00	0.99	0.98–1.0
G-P	4-3A	1D	4	1.0	29.4	0.01	0.95	0.91–0.98
G-P	3-50	1A	5	8.9	17.8	0.01	0.56	0.55–0.57
G-P	3-50	1B	5	3.3	26.2	0.02	0.83	0.83–0.84
G-P	3-53	2A	15	5.4	23.1	0.00	0.73	0.53–0.99
G-P	3-53	2A core	10	7.3	20.2	0.00	0.64	0.53–0.77
G-P	3-53	2A rim	5	1.5	28.9	0.00	0.92	0.83–0.99

Zone abbreviations: G = garnet, G-P = garnet-pyroxene, X_{Ad} = mole fraction andradite in andradite-grossularite solid solution.

growth. The pyroxene is commonly altered to a fine-grained mixture of amphibole, calcite, and quartz. Small, infrequent vugs, lined with coarser euhedral garnet crystals, are filled with calcite and quartz and may contain minor amounts of chlorite, epidote, and pyrite. Overgrowths and large patches of glassy yellow-brown garnet are locally abundant. This garnet contains little or no pyroxene and is associated with calcite and quartz vug fillings with sparse pyrite and chalcopyrite and without epidote or chlorite. As the hanging-wall skarn is approached, rare veinlets of pink anisotropic garnet, up to 5 mm wide, cross-cut both the early buff and later yellow-brown garnet. The final vein fillings consist of isotropic brown garnet, calcite, and rare quartz with a few grains of chalcopyrite and pyrite. These garnet age relations are unambiguous mappable features and are illustrated compositionally by samples 3–6 (Fig. 7) and 3–12A (Figs. 6A and 7).

Microprobe analyses of selected assemblages from three samples of the garnet zone are summarized in Figure 7. The average composition of four pyroxene grains is Hd_{12}. Wide compositional variation within single crystals is unsystematic and may in large part be due to partial equilibration with later fluids which deposited garnet alone. For example, sample

TABLE 5. Partial Microprobe Analyses of Pyroxene (expressed as wt %)

Zone	Sample no.	Grain no.	No. anal.	Al_2O_3	tot Fe as FeO	MgO	X_{Hd}	Range in X_{Hd}
G	4-4	3-B	6	0.15	5.6	12.8	0.20	0.16–0.25
G	3-6	1-C	2	0.11	3.3	16.1	0.10	0.09–0.12
G	3-6	1-D	4	0.65	0.32	19.7	0.01	0.004–0.02
G	3-6	1-E	4	0.07	2.8	16.1	0.09	0.07–0.11
G	3-12A	3-A	9	0.03	4.2	15.5	0.13	0.04–0.23
G-P	4-3A	1-E	6	0.02	10.1	11.2	0.34	0.32–0.41
G-P	4-3A	1-F	6	0.06	10.8	10.4	0.37	0.35–0.40
G-P	3-50	1-D	4	0.04	11.1	9.9	0.39	0.35–0.42
G-P	3-50	1-G	5	0.03	11.2	9.5	0.40	0.37–0.45
G-P	3-53	1-A	7	0.30	0.17	19.2	0.005	0.002–0.006
G-P	3-53	1-B	6	0.11	13.3	8.2	0.48	0.41–0.54
G-P	3-53	2-B	6	0.08	12.1	9.1	0.43	0.37–0.51
P	3-55	1-A	7	0.21	13.4	8.2	0.48	0.39–0.57
P	3-55	1-B	5	0.12	14.5	7.5	0.52	0.43–0.60
P	3-18	1-A	6	0.19	12.9	8.9	0.45	0.44–0.50
P	3-18	2-A	7	0.18	13.3	8.7	0.46	0.44–0.50
M	3-72A	1-A	8	0.16	15.2	6.7	0.56	0.51–0.61
M	3-72A	1-B	6	0.27	6.8	13.1	0.23	0.14–0.37

Zone abbreviations: G = garnet, G-P = garnet-pyroxene, P = pyroxene, M = marble. X_{Hd} = mole fraction hedenbergite in diopside-hedenbergite solid solution.

3–6 contains early anistropic garnet cores (Ad_{38}) which contain pyroxene inclusions ranging in composition from $Hd_{0.4}$ to Hd_2. Where the pyroxene grains extend beyond the early garnet crystals and are overgrown by isotropic yellow-brown andradite (Ad_{100}), their composition changes to Hd_{7-11} in patchy areas concentrated along grain boundaries. Other pyroxene grains which are wholly surrounded and largely replaced by pure andradite (sample 3–12A) may show an unsystematic range in composition from Hd_4 to Hd_{23}.

Early buff garnets are either relatively homogeneous in composition (sample 4-4, with a range of Ad_{33-41}) or are zoned from aluminum-rich cores to iron-rich rims (sample 3–6, zoned from Ad_{34} to Ad_{73}). The more iron rich bands are isotropic, whereas the more aluminum rich bands tend to be anisotropic. Yellow-brown andradite (Ad_{100}) overgrowths (Figs. 8D, 8E, and 8F) may contain thin anisotropic bands of Ad_{84-90}. The thin garnet veinlets which cut the buff and yellow-brown garnet near the contact with the hanging-wall skarn contain pink anisotropic garnet with an average composition of Ad_{61} and a final vein filling with the composition Ad_{98} (sample 3–12A, Figs. 6A and 7).

Two distinct cycles of garnet growth are indicated by the above data. The first cycle, represented by the buff and yellow-brown garnets, started at about Ad_{30} and evolved to pure andradite. During this first cycle, pyroxene growth terminated as garnets reached a composition of about Ad_{50}. The second garnet cycle, represented by the veinlets, started at a higher iron content of about Ad_{50} and evolved to pure andradite. Pyroxene did not form during the second cycle.

Garnet-pyroxene zone: The central zone of the hanging-wall skarn, which at the northern end of the MVM is in contact on the east with the garnet zone, consists predominantly of garnet, pyroxene, and sulfides (Table 1, MVM-4, MVM-2). It has a very different aspect when compared with the garnet footwall zone: relic bedding is absent, grain sizes and sulfide abundance increase abruptly, and dark-green, coarsely bladed pyroxene appears with brown garnet. Maximum chalcopyrite deposition occurred in this mixed garnet-pyroxene zone. Total sulfide abundance is around 15 to 20 percent and the chalcopyrite/pyrite ratio approximates 0.3 in the central portion of the zone and decreases to 0.1 in the outer transition to the pyroxene zone. Pyrite is disseminated throughout and shows no preference for a particular silicate assemblage, although it is locally more abundant in pyroxene than in cross-cutting garnet. Chalcopyrite, invariably accompanied by pyrite, occurs in direct association with late isotropic garnet and calcite in the central portion of the zone, and with isotropic garnet, amphibole, and calcite in the outer transition zone. Chalcopyrite rarely occurs in direct contact with pyroxene.

Although the relative proportion of garnet and pyroxene is extremely variable in hand specimen, there is an overall decrease in the garnet/garnet + pyroxene fraction from 0.75 in the central portion of the zone to 0.25 in the outer portion. Anhedral pyroxene inclusions, 0.1 to 1.0 mm in size, are concentrated in the cores of anistropic brown garnet crystals which average 1 to 2 mm in diameter. This early assemblage, which constitutes some 60 to 80 percent of the total rock, often occurs as fragments a few centimeters in size cemented by a coarse matrix of pyroxene and garnet (Fig. 6B). The pyroxene crystals grew outward from the fragments and characteristically attained lengths of 1 to 3 mm. Zonal anisotropic banding in the garnet associated with the euhedral pyroxene also indicates growth outwards from the walls of the fragments. The final matrix filling generally consists of unzoned isotropic garnet without pyroxene and associated with calcite, quartz, and sulfides. This final garnet-sulfide generation also occurs as cross-cutting veins up to 5 cm wide, and late isotropic garnet preferentially replaces large pyroxene crystals enclosed in anisotropic garnet (Figs. 8G, 8H, and 8I).

The boundary between the garnet-pyroxene zone and the pyroxene zone is gradational and marked by the gradual disappearance of the late garnet-chalcopyrite association and by a gradual decrease in garnet/pyroxene ratios in both wall rock and veins. Amphibole appears in association with isotropic garnet envelopes on chalcopyrite grains. Anisotropic garnet is largely restricted to garnet-pyroxene veins which cross-cut pyroxene-calcite skarn. Rare, thin veinlets of isotropic garnet with chalcopyrite and pyrite cross-cut the garnet-pyroxene veins; abundant chalcopyrite is generally concentrated at the point where these veinlets enter the pyroxene wall rock, and the associated silicate changes from garnet to amphibole (Fig. 6C). These veinlets reflect the overall MVM pattern in which maximum chalcopyrite deposition occurred between the garnet zone and the pyroxene zone. They also conclusively demonstrate the direct genetic association of chalcopyrite with: (1) garnet, (2) garnet + amphibole, and (3) amphibole, on proceeding out toward marble. All three of these ore-bearing assemblages resulted from the replacement of earlier pyroxene or pyroxene + garnet assemblages.

Coarse-grained pyroxenes in the garnet-pyroxene zone are considerably more iron rich than pyroxenes in the garnet zone. The average composition of six pyroxene grains from three samples (4–3A, 3–50, and 3–53) is Hd_{40} (Fig. 7). The average iron con-

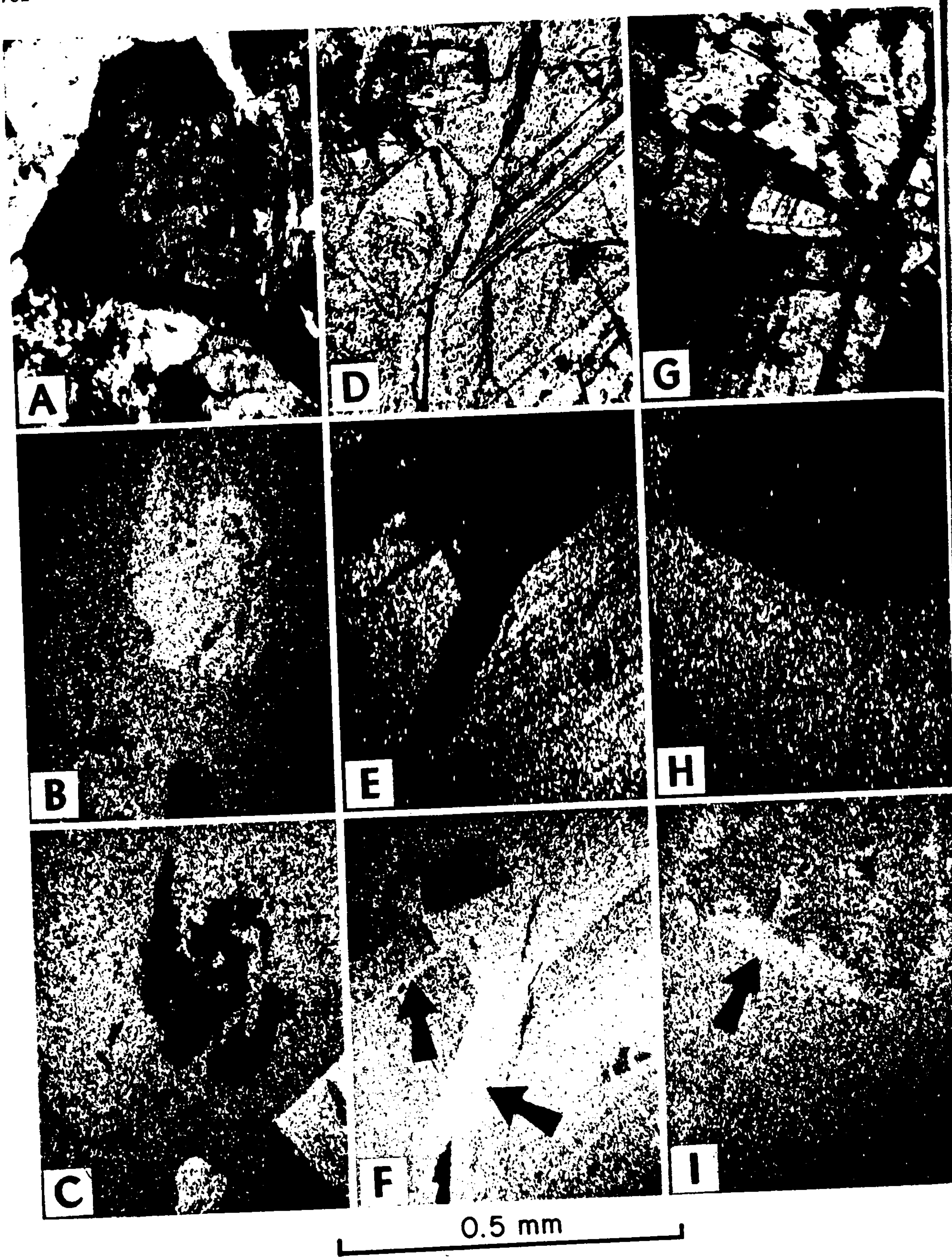

Zone	Sample
G-P	3-50
G-P	3-50
G-P	3-50
P	3-55
M	3-72.

Zone abbreviations: (
ferrotremolite solid solu

tent increases syster
skarn center line or
ratios, from Hd_{36} ir
to Hd_{45} in the outer
Early anisotropic
pyroxene is generall
This composition ra
garnet in veins whic
is probable that the
the hanging-wall sk
footwall skarn. If
pyroxene crystals a
equilibrium with co
and if the garnet-p
footwall skarn are
evident that anisotr
pyroxene display a
toward marble.
Late isotropic ga
and replacing pyro
Ad_{83} to Ad_{100}. Py
by this garnet show
content. For exam
pyroxene crystal of
rounded by garnet
pyroxene grain of
originally enclosed
Ad_{99}.

FIG.
sociatio
A. M
zone. (
B. X
average
C. X
lower r
D. M
E. X
Al rich
F. F
grown
recogni
G. M
and pa
skarn,
H. A
Al rich
I. F
charact

TABLE 6. Partial Microprobe Analyses of Amphibole (expressed as wt %)

Zone	Sample no.	Grain no.	No. anal.	Al_2O_3	tot Fe as FeO	MgO	X_{Ft}	Range in X_{Ft}
G-P	3-50	1-C	5	0.52	14.0	13.8	0.36	0.34–0.39
G-P	3-50	1-E	8	1.1	14.0	13.1	0.38	0.34–0.39
G-P	3-50	1-F	5	0.54	13.8	13.4	0.37	0.36–0.37
P	3-55	1-C	8	0.29	15.7	11.5	0.43	0.39–0.46
M	3-72A	1-D	6	0.25	4.8	20.4	0.12	0.11–0.12

Zone abbreviations: G-P = garnet-pyroxene, P = pyroxene, M = marble. X_{Ft} = mole fraction ferrotremolite in tremolite-ferrotremolite solid solution.

tent increases systematically with distance from the skarn center line or with decreasing garnet/pyroxene ratios, from Hd_{36} in the central portion of the zone to Hd_{45} in the outer transition to the pyroxene zone.

Early anisotropic garnet associated with coarse pyroxene is generally zoned from Ad_{52} to about Ad_{77}. This composition range is similar to that of the pink garnet in veins which cut the garnet footwall, and it is probable that these veins represent an overlap of the hanging-wall skarn mineralization onto the early footwall skarn. If the compositions of the coarse pyroxene crystals are taken to represent chemical equilibrium with contemporaneous anistropic garnet, and if the garnet-pyroxene compositions from the footwall skarn are also considered, then it becomes evident that anisotropic garnet and contemporaneous pyroxene display a mutual increase in iron content toward marble.

Late isotropic garnet associated with chalcopyrite and replacing pyroxene varies in composition from Ad_{83} to Ad_{100}. Pyroxene which is largely replaced by this garnet shows no significant increase in iron content. For example, sample 4-3A contains a coarse pyroxene crystal of composition Hd_{34} which is surrounded by garnet of composition Ad_{55}. Nearby, a pyroxene grain of composition Hd_{37} which was originally enclosed in Ad_{55} is largely replaced by Ad_{99}.

Rare pyroxene crystals in the transition to the pyroxene zone and in the pyroxene zone itself contain core zones with a different extinction angle than the rims. One such grain (sample 3–53) contains a core of composition $Hd_{0.5}$ irregularly rimmed by Hd_{48} (Figs. 8A, 8B, and 8C). Such low-iron cores are presumed to represent an early stage of pyroxene growth which was largely obliterated within the central skarn zones, but which is preserved in the marble contact zone.

Actinolite associated with Ad_{83} and chalcopyrite along veinlets in pyroxene (sample 3–50, Figs. 6C and 7) has approximately the same Fe/Mg ratios (Ft_{34-39}) as the associated pyroxene.

Pyroxene zone: The outermost silicate zone at the MVM consists largely of coarse, dark-green pyroxene (Hd_{49}) and pyrite (Table 1, MVM-3). Large patches of calcite are of common occurrence, and these may contain minor amounts of quartz and magnetite pseudomorphous after specular hematite. Local spots and disseminations of chalcopyrite are present, and these invariably contain coarse needles of actinolite (Ft_{39-46}), some of which have replaced early pyroxene, especially where the latter abuts against chalcopyrite (Fig. 6D). The associated pyroxene, which rarely is in direct contact with chalcopyrite, displays a wide range in composition, from Hd_{39} to Hd_{60} (sample 3–55). Pyroxene associated

FIG. 8. Microphotographs and electron beam scanning pictures of garnet and pyroxene associations.

A. Microphoto of pyroxene grain from specimen 3–53, hanging-wall skarn, garnet-pyroxene zone. Crossed nicols reveals core zone (gray) with different extinction angle than rim (black).

B. X-ray scan displays intensity of Mg $K\alpha$ radiation from area of Figure 8A. Core zone averages $Hd_{0.5}$, whereas rim averages Hd_{48}.

C. X-ray intensity display of Fe $K\alpha$ radiation from area of Figure 8A. Pyrite grains in lower right are recognized by their high Fe content.

D. Microphoto of garnets from specimen 3–6, footwall skarn.

E. X-ray intensity display of Al $K\alpha$ radiation from the area of Figure 8B reveals relatively Al rich zoned garnet (Ad_{84-78}) in lower half of picture.

F. Fe $K\alpha$ radiation from area of Figure 8B reveals Fe-rich garnet (Ad_{100}) which has overgrown and veined (arrows) earlier zoned garnet. Pyroxene grain in upper left (black) is recognized by its low Fe content.

G. Microphoto of pyroxene crystal (white) enclosed in anisotropic garnet (banded, gray) and partially replaced along rim by isotropic garnet (black). Specimen 4-3A, hanging-wall skarn, garnet-pyroxene zone. Crossed nicols.

H. Al $K\alpha$ radiation from area of Figure 8C reveals that the enclosing garnet is relatively Al rich and homogeneous (Ad_{51-57}).

I. Fe $K\alpha$ radiation from area of Figure 8C reveals that the isotropic garnet (arrow) is characterized by relatively high Fe content (Ad_{92-98}).

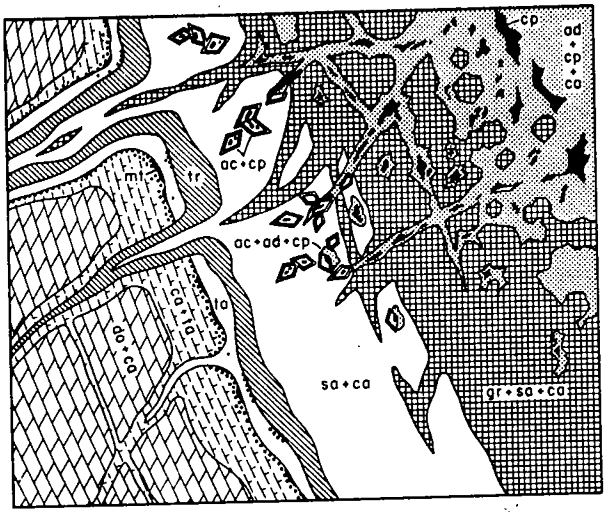

FIG. 9. Schematic summary of paragenesis and zoning, hanging-wall skarn. Mineral abbreviations are listed in Table 3. Scale is variable. Pyrite occurs throughout.

with calcite or calcite plus pyrite is significantly more homogeneous and less iron rich (Hd_{44-50}, sample 3–18).

Marble contact zone: Beyond the edge of the massive pyroxene skarn, pyroxene veins extend into the dolomite-calcite marble. These veins, which may be a few centimeters to a meter wide, consist largely of irregular, alternating bands of coarse-grained dark-green pyroxene (Hd_{56}) and fine-grained pale-green pyroxene (Hd_{23}). The latter bands do not contain calcite. A layer of coarse pyroxene generally occupies the vein center and is associated with calcite patches up to 1 cm in size. Anisotropic garnet crystals are also rarely present in the vein centers, especially near the pyroxene zone contact. Pyrite is randomly disseminated throughout the pyroxene in amounts ranging from 1 to 5 percent, and magnetite, generally associated with calcite-pyroxene, is present in trace amounts.

Pale-green to black envelopes, 1 to 10 mm wide, separate the pyroxene from the dolomitic marble (Fig. 9). These envelopes consist of sequential layers, with knife-edge boundaries, of (1) tremolite, (2) talc, (3) magnetite, and (4) calcite, out toward marble. The talc and magnetite zones are absent in some vein halos. The tremolite zone consists of radial aggregates and interlocking needles of tremolite, 0.05 to 0.5 mm in length (Ft_7). It contains sparse amounts of pyrite and calcite and rare concentrations of magnetite grains at the inner contact with pyroxene. The talc zone is monomineralic, and consists of felted aggregates up to 0.4 mm long arranged at right angles to the zone boundaries. The magnetite zone may be represented by a single layer of magnetite grains 0.05 mm in diameter separating talc from talc-calcite, or it may constitute a zone up to 1 mm wide in which magnetite grains are disseminated in a microcrystalline aggregate of calcite and talc. Minor, coarse tremolite needles are also present, and flaky aggregates of chlorite are aligned parallel to the vein boundary. The outermost calcite zone consists predominantly of 0.1- to 0.2-mm domains of finely recrystallized 0.01-mm turbid calcite grains which contain minor talc and chlorite. The contact with dolomitic marble, which contains dolomite, calcite, and sparse chlorite, is sharp.

Some inner zone minerals transgress outer zones along fractures. In a few cases, talc veinlets extend through magnetite into the calcite zone. More commonly, tremolite cuts across both the talc and the magnetite zones and extends out into dolomitic marble where it generates calcite-tremolite envelopes. Locally, tremolite is in direct contact with both calcite and dolomite. These relations indicate that: (1) the magnetite zone is an early feature that was locally overgrown during continued talc formation and did not continue to form as talc moved out; and (2) talc, though it continued to form after magnetite had stopped depositing, is also early relative to some of the tremolite. The talc and magnetite zones did not constitute part of the mineral zoning sequence during the later stages of development of the pyroxene-tremolite veins.

The critical assemblages which formed in the pyroxene vein envelopes are: (1) diopside-tremolite-calcite; (2) tremolite-talc-calcite; and (3) tremolite-dolomite-calcite. The dominant mode of occurrence of these phases on the scale of several millimeters, however, is as one- or two-phase assemblages in the pyroxene, tremolite, and talc zones, and the three-phase assemblage tremolite-talc-calcite (plus magnetite and/or chlorite) in the magnetite and calcite zones. Diopside is nowhere in contact with talc or dolomite, and talc does not occur with diopside or dolomite. Calcite is present throughout.

On the far edge of the dolomitic marble zone, where it is particularly well exposed in crosscuts on the 400 level, silicate vein centers are composed entirely of coarse-grained, pale-green to white tremolite. Envelopes are similar to those previously described. No examples of pyroxene veins cutting tremolite veins were noted. And, though no veins were noted in which the pyroxene progressively gives way to tremolite in the vein centers, such a relation would seem to be probable.

Summary: The early hornfels stage of contact metasomatism is represented at the MVM by the footwall skarn. In this zone, low-iron pyroxene (Hd_{12}) and relatively aluminum rich garnet (Ad_{30-50}) formed together and were later overgrown by more iron rich garnet without pyroxene. During hanging-wall skarn formation, the footwall skarn was veined by a second cycle of garnet deposition which evolved from Ad_{50} to Ad_{100} and was locally accompanied by pyrite and chalcopyrite.

On the marble side of the hanging-wall skarn, calcite-talc-magnetite formed early during the silication-mineralization cycle and was replaced on the veinward side by relatively low iron tremolite (Ft_7). Talc-calcite or tremolite-dolomite-calcite continued to form from dolomitic marble as the tremolite veins extended beyond the magnetite zone. Pyroxene formation was initially characterized by abrupt rhythmic fluctuations in grain size and composition, but as the silication process continued pyroxene compositions became relatively homogeneous in the range Hd_{50-60}. Early, low-iron cores were rarely preserved. The tremolite-dolomite-calcite assemblage presumably continued to form on the marble contact as it was replaced on the skarn side by pyroxene-calcite. Sparse amounts of magnetite and local specular hematite continued to form during this stage, but the evidence on pyrite is inconclusive.

As early garnet (Ad_{55}) began to form on the veinward side, the iron content of the associated pyroxene progressively dropped from Hd_{45} to Hd_{33}, magnetite-hematite disappeared, and pyrite appeared in abundance. Continued anisotropic garnet growth (Ad_{60-80}) was accompanied by fracturing and local brecciation of both pyroxene-pyrite and garnet-pyroxene-pyrite and an increase in garnet/pyroxene ratios. Calcite and local calcite-quartz were deposited interstitially to final breccia fillings of coarse euhedral garnet without pyroxene. Early anisotropic garnet does not extend beyond the outer edge of the pyroxene zone, but it is locally present in pyroxene vein centers in the marble zone. This relation suggests that early garnet was part of the process of zoned skarn formation and that its growth on the veinward side was coincident in time with the continued outward growth of the pyroxene, tremolite, and talc-calcite or tremolite-dolomite-calcite zones.

Chalcopyrite deposition, accompanied by additional pyrite, commenced with the final stages of silication in the hanging-wall skarn. The vast majority of the chalcopyrite is directly associated with andradite-calcite overgrowths and veins in the central portion of the garnet-pyroxene zone. Pyroxene growth in this portion of the skarn had terminated, and pyroxene crystals were partially replaced by andradite. In the pyroxene zone, minor chalcopyrite deposition was accompanied by actinolite rather than andradite. This process also resulted in the partial destruction of pyroxene. Andradite-actinolite-chalcopyrite-calcite assemblages are rare and spatially restricted to the outer garnet-pyroxene zone.

Petrogenesis

Contemporaneity of zone development

The identification of relative-age criteria applicable to zonally arranged alteration has been elegantly treated by Meyer and Hemley (1967): ". . . the simple geometry of the banded zonal pattern is unobligingly ambiguous" (p. 181). Two specific field relations at the MVM shed light on the problem:

(1) Garnet-pyroxene veins cut pyroxene rock. This fact implies that the garnet-pyroxene zone encroached on the pyroxene zone, but it does not require the entire garnet-pyroxene zone to be later than the entire pyroxene zone. The two zones could have developed contemporaneously, a choice supported by the fact that nowhere does the garnet-pyroxene zone cut across the pyroxene zone and encroach directly onto unsilicated marble—the two zones are ubiquitously concentric (cf. Meyer and Hemley, 1967).

(2) TrCc veins cut the outer Ta and TaMtCc zones and encroach directly onto unsilicated marble, implying that they formed after TaCc formation had terminated, although elsewhere in the system, presumably at lower T or higher X_{CO_2}, TaCc may still have been forming.

Main skarn stage: Notwithstanding the above ambiguities, it is reasonable to conclude that the alteration pattern of the MVM hanging-wall skarn resulted from essentially contemporaneous development of zones which migrated outwards, with only locally over-ridden or absent intermediate zones. Such a model is maintained by many students of skarn deposits (e.g., Titley, 1961) and has been applied to the formation of calc-silicate bands in middle- to upper-amphibolite facies metamorphism (Vidale and Hewitt, 1973).

A second interpretation for zonal patterns of this type is that the innermost zone formed first and that solutions flowing through it superimposed later outer zones. In this interpretation, each zone forms directly by replacement of marble and once formed does not migrate. Bartholomé and Evrard (1970) apply this mechanism to the zoned sequence Mt-ilvaite-Hd-marble at Temperino, Italy, although the lack of field and petrographic data weakens their conclusion. Cermignani and Anderson (1973), in a very well documented study, conclude that zoned Di-Tr-Cc veins in Grenville dolomites near Tweed, Ontario, resulted from early formation of diopside followed by fracturing and a change in T-X_{CO_2} allowing TrCc to form at the contact between diopside and dolomite. These examples underline the need for detailed field and petrographic observations on which to establish models of skarn formation.

Inferring contemporaneity of zone development

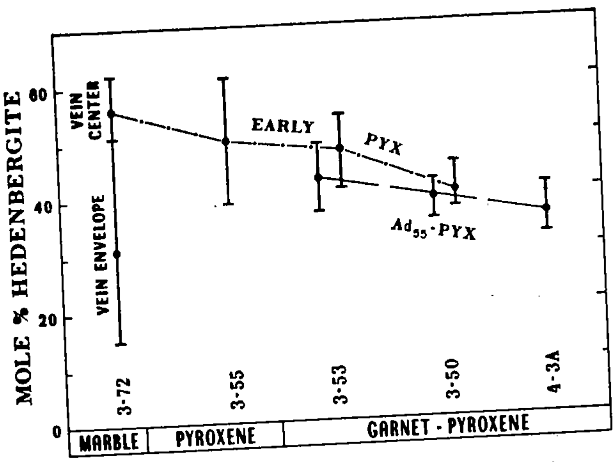

FIG. 10. Plot of mean compositions (dots) and range (vertical bars) of hedenbergite content in pyroxenes from the MVM. Samples are from the northern end of the mine and are arranged to illustrate composition trends over a distance of 100 m along a line subparallel to the hanging-wall skarn center line. Dash-dot line connects pyroxenes which predate garnet deposition. Dashed line connects later pyroxenes which are contemporaneous with grandite deposition.

implies nothing about the relative ages of phases *within* the individual zones. For example, as new, relatively iron rich pyroxene formed in the marble, was the pyroxene in the skarn (1) adjusting its composition to the existing fluid composition gradients, or (2) was it effectively nonreactive? The former implies that all pyroxenes in the pyroxene zone are contemporaneous and that their present compositional variations across the zone reflect the thermal and chemical gradients in the *final increment* of solution. The latter case implies that pyroxenes in the marble are the youngest, and that the present compositional variations reflect the changes *with time* of the thermal and chemical characteristics of the fluid. The pattern within the pyroxene zone is ambiguous and cannot be resolved on the basis of its geometry alone.

The garnet-pyroxene zone is less ambiguous because of the sequential appearance of pyroxene, then garnet-pyroxene, and finally garnet alone. The distinct compositional changes exhibited by garnet aid in establishing the sequence of mineral formation within the zone. The lack of equilibration of early pyroxene with later solutions depositing garnet-pyroxene is illustrated by samples 3–53 and 3–50 (Fig. 10) and may be due largely to the restriction of fluids to open fractures.

Ore stage: Concentric zones are not always developed in the garnet-pyroxene zone. Latest $Ad_{100}CpCc$ assemblages are not restricted to $Ad_{55}Hd_{40}$ envelopes or patches, but rather cut across these and encroach directly onto Hd_{50} rock. Ad_{100} tends to replace pyroxene in the $Ad_{55}Hd_{40}$ assemblage (Figs. 8G, 8H, and 8I), but where it impinges on Hd_{50}, pyroxene is altered to actinolite. The apparent compatibility of Ad with Hd_{40} and its incompatibility with Hd_{50} could reflect a T-X_{CO_2} control.

A cogenetic association of garnet and sulfides is generally not indicated by skarn studies, although local occurrences of sulfide-magnetite veinlets with garnet envelopes in marble at Ely, Nevada, have been described by James (1976). Disseminations of chalcopyrite-pyrite in garnet-pyroxene are noted in numerous deposits, but such textures could result from late sulfide deposition from pore fluids which did not alter the garnet-pyroxene. The present study supplies evidence that in the central skarn zone chalcopyrite deposition occurred during late andradite veining and replacement of salite by andradite, whereas in the outer zone chalcopyrite deposition was accompanied by alteration of salite to actinolite. The contemporaneity of these two environments is suggested by the veinlets illustrated in Figure 6C.

Phase equilibria

The progressive changes in mineral assemblages which characterize skarns may result from gradients in T-X_{CO_2} and/or gradients in the chemical potentials (μ) of nonvolatile components. Although it is virtually impossible to uniquely specify such variables for polycomponent rocks of very few phases, certain dependencies among variables may be determined. For example, an isothermal gradient in X_{CO_2} has been suggested as the zoning control in micaceous limestones in south-central Connecticut (Vidale and Hewitt, 1973). In this example, the system was considered isochemical except for CO_2 and H_2O, and the boundaries between zones represent isobarically univariant T-X_{CO_2} reaction curves. Mineral zoning sequences in iron-rich calcium exoskarns have been discussed by Burt (1974) in terms of diffusion-controlled gradients in $\mu_{SiO_2}\mu_{FeO}$, and μ_{CaO} at externally controlled T, P, μ_{O_2}, and μ_{CO_2} (the latter variables define the skarn facies). Burt concludes that several different zoning sequences may be possible within a given facies and, conversely, that the same zoning sequence could form within two different facies.

The MVM skarn is more complex than the above examples, and the analysis of phase equilibria is hampered by the lack of experimental and thermochemical data for phases of variable composition. The zoned veins of the marble contact are interpreted below, as a first approximation, on the basis of equilibria in the system CaO-MgO-SiO_2-H_2O-CO_2. However, the addition of iron to the system, as in the pyroxene and garnet-pyroxene zones, causes the appearance of new phases and introduces compositional variation in pyroxene and amphibole. Isobaric univariant equilibria will shift from their Mg end member positions and become functions not only of T

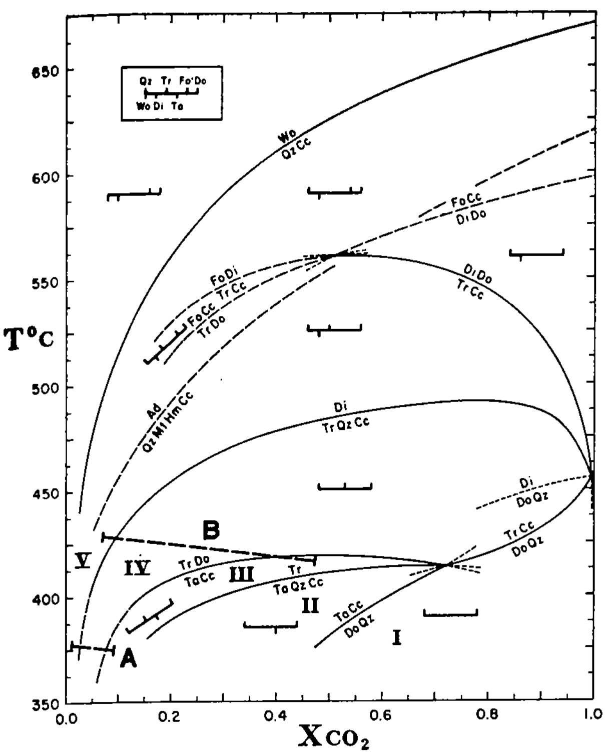

FIG. 11. T-X_{CO_2} diagram at 1,000 bars $P_{H_2O} + P_{CO_2}$ for calcite-bearing equilibria in the system CaO-MgO-SiO_2-H_2O-CO_2, from Slaughter and others (1975) and Greenwood (1967). The approximate position of the andradite-terminal reaction is from Taylor and Liou (1975). Abbreviations in Table 3.

and X_{CO_2} but also of f_{O_2}. The interpretation in this case is based on writing appropriate chemical reactions which illustrate the interdependence of intensive variables.

μ_{Si}-μ_{Mg} $-X_{CO_2}$ *gradients, marble contact:* The definitive experimental studies in the system CaO-MgO-SiO_2-H_2O-CO_2 are those of Skippen (1967, 1971, 1974), Gordon and Greenwood (1970), and Slaughter et al (1975). Recent compilations and comparisons are supplied by Kerrick (1974) and Slaughter et al. (1975). Figure 11 summarizes T-X_{CO_2} equilibria for the calcite-bearing portion of the system at 1,000 bars total pressure and includes the CcQz = Wo curve from Greenwood (1967) and the andradite-terminal reaction from Taylor and Liou (1975). No isobarically univariant or invariant assemblages (X_{CO_2} buffers) appear in this system at the MVM. All assemblages have an isobaric variance of two or greater, suggesting that the system was open to both CO_2 and H_2O.

The presence of calcite throughout the zonal sequence in early vein envelopes implies that μ_{CaO} was a function of μ_{CO_2}, and the narrow width of these veins suggests that metasomatism occurred at constant temperature. For these conditions, the sequence of phase assemblages may be interpreted in terms of isothermal gradients in X_{CO_2}, μ_{Si}, and μ_{Mg} (Fig. 12) induced by reaction of dolomitic wall rocks with a metasomatic fluid characterized by relatively low μ_{Mg} and close to saturation with quartz. The sequence of two-phase assemblages represents the successive attainment of appropriate μ-values and not the crossing of isobarically univariant T-X_{CO_2} curves. The phase path for calcite saturation within a given divariant T-X_{CO_2} field is unique. The lack of correspondence of any such paths in Figure 12 with the complete MVM early vein sequence requires that X_{CO_2} decreased with time or toward the vein center. Portions of the early vein zoning appear in successive diagrams of Figure 12 from right to left with decreasing X_{CO_2}. The lack of isobarically univariant assemblages makes it impossible to assign a value to the X_{CO_2} gradient, even if the temperature were known. For example, the initial increase in μ_{Si} which led to the replacement of DoCc by TaCc could have occurred in either divariant region II or III (Figs. 11 and 12). However, general limits to the X_{CO_2} gradient can be inferred from the location of divariant fields shown in Figure 11. For maximum temperature conditions (limited by invariant point TrTaDoCcQz at 410°C, 1,000 bars) a minimum X_{CO_2} gradient would be approximately from 0.1 to 0.5 (gradient B, Fig. 12). At lower temperatures the minimum gradient in X_{CO_2} is significantly diminished and could be less than $X_{CO_2} = 0.1$ (gradient A, Fig. 12).

Other MVM assemblages that belong to this system are less instructive than TaCc. These include the assemblages TrCc and TrCcDo which belong to the later vein stage and represent higher temperatures and/or lower X_{CO_2} conditions than the early vein assemblage TaCc (Fig. 11).

Graphical presentation of Fe-Mg assemblages: The variations in phase compositions and assemblages across the skarn zone in terms of the eight-component system Ca-Mg-Fe-Si-O_2-H_2O-CO_2-S_2

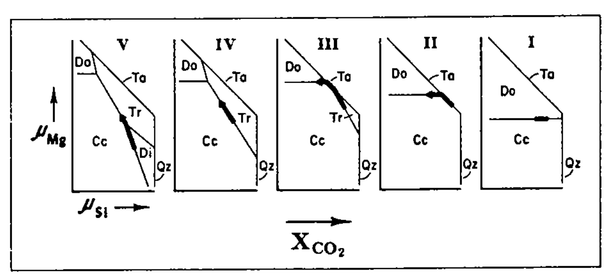

FIG. 12. Isobaric chemical potential diagrams for diffusing components Mg and Si drawn for the five divariant T-X_{CO_2} facies illustrated in Figure 11. Black arrows denote μ-gradients from the center of skarn veins toward the marble contact.

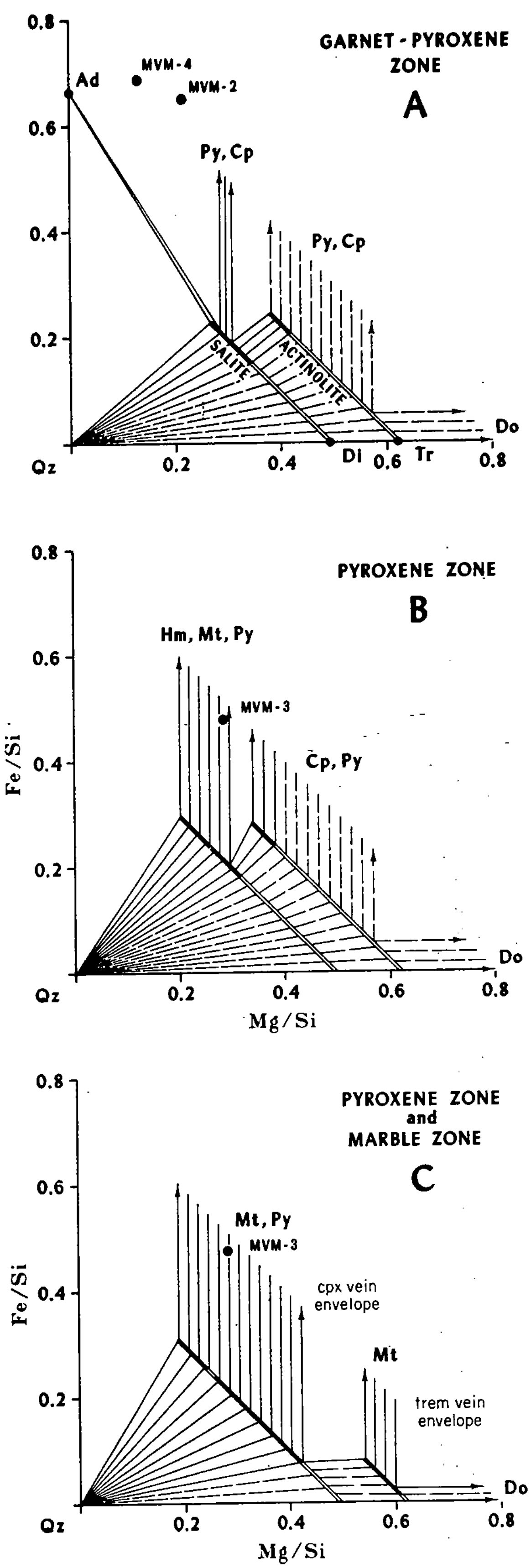

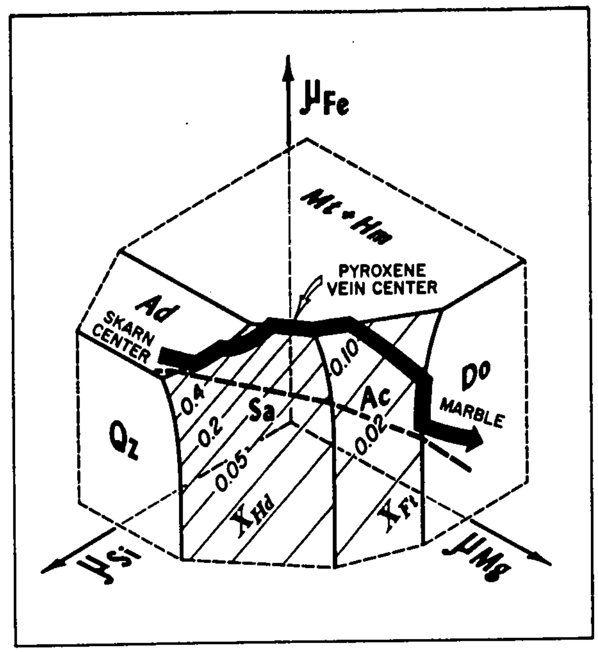

FIG. 14. Chemical potential diagram for diffusing components Fe, Mg, and Si at constant P, T, f_{O_2}, and X_{CO_2}, and with μ_{CaO} controlled by the presence of excess calcite. Contours for mole fraction iron end member in salite and actinolite are schematic. The diffusion paths are discussed in text.

can be summarized by plotting the phases which coexist with excess calcite and fluid onto a Fe-Mg-Si triangle or onto an orthogonal plot of Fe/Si versus Mg/Si. The latter plot has numerous advantages over the former in that it (1) expands the scale of the area of interest (the pyroxene and amphibole series), and (2) is readily transformed into the μ_{Fe}–μ_{Mg} diagram (see Korzhinskii, 1959, p. 90–96).

A set of three Fe/Si-Mg/Si plots is presented in Figure 13. Figure 13A indicates that salite coexisting with AdCcPy should have a higher iron content than salite coexisting with AcCcPy. The lack of any systematic variation of this kind in salite compositions between these assemblages at the MVM indicates that variations in parameters such as T, X_{CO_2}, f_{O_2}, or f_{S_2} were important controls of phase composition. At constant pressure the above parameters control the extent of solid solution and the arrangement and slope of tie lines which define the assemblages. The plots in Figure 13 should therefore be regarded as schematic summaries of the general features of composition and assemblage.

FIG. 13. Fe/Si versus Mg/Si diagrams for calcite-bearing parageneses illustrating phase composition-assemblage data from various zones at the MVM. Solid tie lines represent assemblages recorded at the MVM, whereas dashed tie lines represent other possible, but not recorded, assemblages. The slope of the tie lines, which is reflected in the slope of phase boundaries in the corresponding μ-μ diagrams, is determined by the microprobe analyses. The solid black bars represent the range in composition of solid solutions. Solid circles represent bulk composition of skarn zones from Table 1.

Several n
Figure 13.
with dolom
SaMtCc and
MVM skarı
favored ove
over AdAc(
Certain aspe
by these mi
following se(

Fe-Mg re
zonal patterı
to those usec
system, in wl
ing simultane
chemical poı
may be basec
representing
components,
and at a μ_{CaO}
calcite (Fig.
using analyz
1959). Che
reaction bet
forming solut
and possibly
decreased tov
potentials of
Such a gradi
line in Figur
would consis
AdCc. A pa
tern more clo
chemical pote
such that ph
distances (he

Yet, Figur
zonal minera
tion of indivi
that actinolite
iron enrichme
T and X_{CO_2} ur
Such an iron
the outer pyr
shifts abruptly
contact inwar
gressively less
composition o
part by T-X_{CO}
be discussed i
μ_{Fe}-μ_{Mg} diagra
diagrams are
grams of Fig
conditions of
may be drawn

(1) A decr
vein center to

Several mineral incompatibilities are suggested by Figure 13. For instance, andradite is not compatible with dolomite because of the persistence of the SaMtCc and AcMtCc tie planes. For the conditions of MVM skarn formation, AdSaCc and SaMtCc were favored over AcQzCc; also, SaMtCc was favored over AdAcCc except locally during ore deposition. Certain aspects of the T-X_{CO_2}–f_{O_2} conditions implied by these mineral compatibilities are discussed in the following section.

Fe-Mg reactions: In a simplified sense, the MVM zonal pattern might be explained by a model similar to those used by Burt (1974) in the Fe end member system, in which all zones can be regarded as developing simultaneously as the result of diffusion-controlled chemical potential gradients. Graphical modeling may be based on isobaric chemical potential diagrams representing saturation surfaces for three diffusing components, at constant temperature, X_{CO_2}, and f_{O_2}, and at a μ_{CaO} consistent with the presence of excess calcite (Fig. 14). Such diagrams may be constructed using analyzed mineral compositions (Korzhinskii, 1959). Chemical potential gradients resulted from reaction between dolomite wall rocks and skarn-forming solutions saturated with respect to andradite and possibly quartz. The chemical potential of Mg decreased toward the skarn center, and the chemical potentials of Si and Fe decreased toward the marble. Such a gradient is illustrated by the heavy dashed line in Figure 14. The resulting bimineralic zones would consist of the sequence: DoCc-AcCc-SaCc-AdCc. A path which approximates the MVM pattern more closely involves local or internal control of chemical potentials for some portions of the skarn, such that phase boundaries are followed for short distances (heavy black line, Fig. 14).

Yet, Figure 14 approximates only the general zonal mineralogy and not the variations in composition of individual phases. The above model requires that actinolite and salite both undergo progressive iron enrichment toward the skarn center at constant T and X_{CO_2} until saturation with andradite is reached. Such an iron-enrichment trend is present only in the outer pyroxene vein envelopes, where pyroxene shifts abruptly from Hd_{15} to Hd_{56}. From the marble contact inward, however, the pyroxene becomes progressively less iron rich. This fact suggests that the composition of pyroxene may have been controlled in part by T-X_{CO_2}-f_{O_2} gradients. This possibility may be discussed in terms of Figure 15 which presents μ_{Fe}-μ_{Mg} diagrams projected along the μ_{Si} axis. These diagrams are constructed from the paragenesis diagrams of Figure 13 and represent four different conditions of T-X_{CO_2}. The following conclusions may be drawn:

(1) A decrease in μ_{Fe} and increase in μ_{Mg} from vein center toward marble, at constant T, X_{CO_2}, and

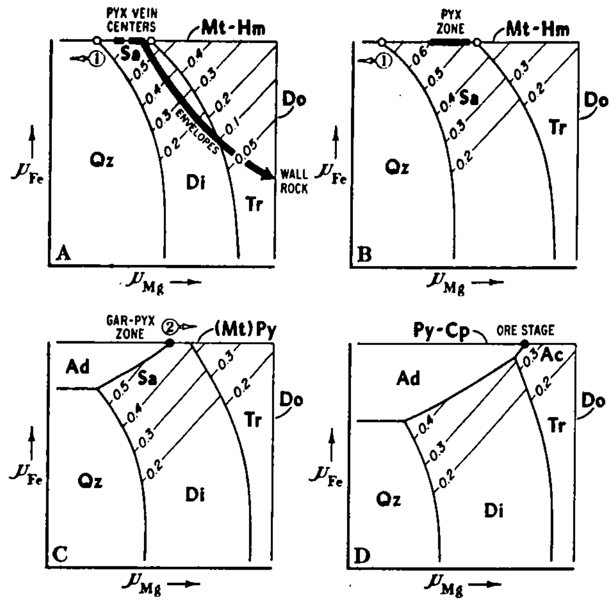

FIG. 15. Schematic chemical potential diagrams projected along the μ_{Si} axis onto the μ_{Fe}-μ_{Mg} plane, at constant P, T, f_{O_2}, and X_{CO_2}. Calcite is present throughout. Contours represent mole fraction of iron end member in pyroxene and amphibole. Arrows on circled numbers indicate direction of shift of invariant points 1 and 2 relative to salite composition contours with increasing T and/or decreasing X_{CO_2}.

μ_{CaO}, could yield the phase zoning and compositional variation in pyroxene and amphibole documented for the marble contact veins which cut the early TaCc-bearing veins (Fig. 15A). Variations in T-X_{CO_2} conditions may have occurred, but such changes may be specified only in the case of appropriately buffered assemblages.

One such assemblage is SaMtHmQzCc (invariant point 1, Fig. 15A), which is locally present near the vein centers. The dependence of salite composition on T, X_{CO_2}, and f_{O_2} can be determined qualitatively by writing the continuous Fe-Mg reaction

$$Sa + Mt + Qz + Cc \leftrightharpoons Sa' + O_2 + CO_2 \quad (1)$$

where Sa′ is more iron rich than Sa. The limiting case for this continuous reaction is the equivalent Fe end member reaction

$$\underset{Mt}{Fe_3O_4} + \underset{Qz}{6\,SiO_2} + \underset{Cc}{3\,CaCO_3} \leftrightharpoons \underset{Hd}{3\,CaFeSi_2O_6} + 3\,CO_2 + \tfrac{1}{2}O_2 \quad (1')$$

Assuming that the activities of solids other than clinopyroxene are equal to unity, the equilibrium constant is

$$K_1 = a_{Hd}^3 f_{CO_2}^3 f_{O_2}^{\frac{1}{2}}$$

where a_{Hd} is the activity of $CaFeSi_2O_6$ in clinopyroxene. If the latter phase is an ideal solution (Mueller, 1961), then

$$X_{Hd} = \sqrt[4]{K_1/(f_{O_2}^{1/2} f_{CO_2}^{3})}$$

where X_{Hd} is the mole fraction of $CaFeSi_2O_6$ in clinopyroxene. This relation indicates that, with f_{O_2} buffered by MtHm, X_{Hd} is an isobarically univariant function of T and f_{CO_2} (or X_{CO_2}); increasing temperature and/or decreasing X_{CO_2} would cause a progressive increase in the iron content of salite in the assemblage SaMtHmQzCc. This result is compatible with a model of decreasing X_{CO_2} toward pyroxene vein centers of the marble contact zone, but cannot be applied to the pyroxene zone as a whole due to the general absence of quartz and the near-constant composition of salite (Fig. 15B).

(2) The decrease in X_{Hd} in the garnet-pyroxene zone may have resulted from a continuous Fe-Mg reaction of the type

$$Sa' + Mt + Cc + O_2 \leftrightarrows Sa + Ad + CO_2 \quad (2)$$

where Sa′ is more iron rich than Sa. This reaction is represented by invariant point (2) in Figure 15C, which represents higher T and/or lower X_{CO_2} than Figures 15A and 15B. The Fe end member reaction equivalent to reaction (2) is

$$\underset{Hd}{18\ CaFeSi_2O_6} + \underset{Mt}{2\ Fe_3O_4} + \underset{Cc}{18\ CaCO_3} + 5\ O_2 \leftrightarrows \underset{Ad}{12\ Ca_3Fe_2Si_3O_{12}} + 18\ CO_2 \quad (2')$$

and

$$K_2 = f_{CO_2}^{18}/a_{Hd}^{18} f_{O_2}^{5}$$

Assuming that clinopyroxene is an ideal solution

$$X_{Hd} = \sqrt[18]{f_{CO_2}^{18}/(K_2 f_{O_2}^{5})}$$

Hence, a gradient toward higher T and/or lower X_{CO_2} would cause a decrease in the iron content of salite in the assemblage AdSaMtHmCc.

(3) The local appearance of the assemblage AdAcPyCc suggests the following isobarically univariant discontinuous reaction:

$$Sa + MtHm + O_2 + CO_2 + H_2O \rightleftarrows Ad + Ac + Cc \quad (3)$$

represented by the change in topology between the μ-diagrams of Figures 15C and 15D. A decrease in T and/or increase in X_{CO_2} at low values of X_{CO_2} favors the AdAcCc assemblage. The stable existence of this reaction depends on the direction of shift of the reaction TrQzCc = Di + CO_2 + H_2O on addition of iron. Taylor and Liou (1975) have demonstrated by experiment that andradite is not stable in the TrQzCc stability field (Fig. 11). A shift of the diopside-terminal reaction toward higher temperatures on addition of iron is therefore required for the stable existence of the assemblage AdAcCc. Such a shift is suggested by Thompson (1975b) on the basis of Fe/Mg distribution between naturally occurring clinopyroxenes and low-Al calcic amphiboles.

In summary, increasing temperature and/or decreasing X_{CO_2} toward the skarn center may have been recorded by the composition of salite. The exact path, and the changes in salite composition or appearance of new phases, would ultimately depend on the extent of equilibrium between wall rock and fluid. Equilibrium may have been maintained for a period of time at invariant point 2, Figure 15C, due to abundance of salite and relatively high density of fractures. Garnet and salite formed contemporaneously and the trend toward iron enrichment in salite was reversed. Evidence cited earlier for restriction of fluids to open fractures and lack of complete reconstitution of early phases indicates that the fluid eventually became chemically insulated from the wall rocks by newly formed garnet. The effectiveness of salite as a buffer was reduced, and the composition of the fluid shifted abruptly into the garnet field. At this stage, or slightly later and at lower temperatures, the assemblage AdAcCc became stable relative to SaMtHm (reaction 3). The appearance of andradite and the shift in compatibilities marked the beginning of major ore deposition. This relationship suggests that crystallization of large amounts of iron-rich garnet caused the decrease in Fe/Cu ratio in the ore fluid which led to saturation with chalcopyrite.

Bulk composition gradients

The bulk compositions of the various skarn zones presented in Table 1 were determined by chemical analysis of channel samples from the 300 level (Fig. 4). The abundance of brecciation and fracturing followed by deposition of later silicates, often as apparent open-space fillings, suggests that if volume loss occurred during initial stages of silication it was expressed by an increase in porosity at constant bulk volume. Uncertainties with regard to such volume changes make calculations of chemical gains and losses of questionable value. The gross variation in chemical composition of the skarn is therefore presented in Figure 16A in terms of g/cc of oxides present. With the assumption of constant volume, gains and losses may be readily determined from this figure. The composition of the nonsulfide portion of the skarn was calculated by subtracting S and

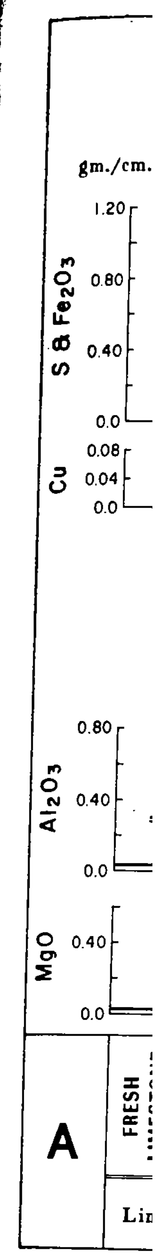

Fe in sulfides
recalculating
of 3.1. Thus
mate composi
deposition.
The most in
is the significa
from a simpl

) on addition
lemonstrated
table in the
shift of the
ier tempera-
uired for the
:Cc. Such a
75b) on the
naturally oc-
: amphiboles.
: and/or de-
er may have
salite. The
composition
ultimately de-
een wall rock
n maintained
, Figure 15C,
y high density
ed contempo-
enrichment in
earlier for re-
l lack of com-
indicates that
insulated from
t. The effec-
uced, and the
uptly into the
y later and at
dAcCc became
3). The ap-
compatibilities
position. This
ation of large
he decrease in
d to saturation

ous skarn zones
ed by chemical
300 level (Fig.
and fracturing
es, often as ap-
that if volume
silication it was
at constant bulk
to such volume
nical gains and
oss variation in
s therefore pre-
g/cc of oxides
constant volume,
letermined from
nonsulfide por-
ubtracting S and

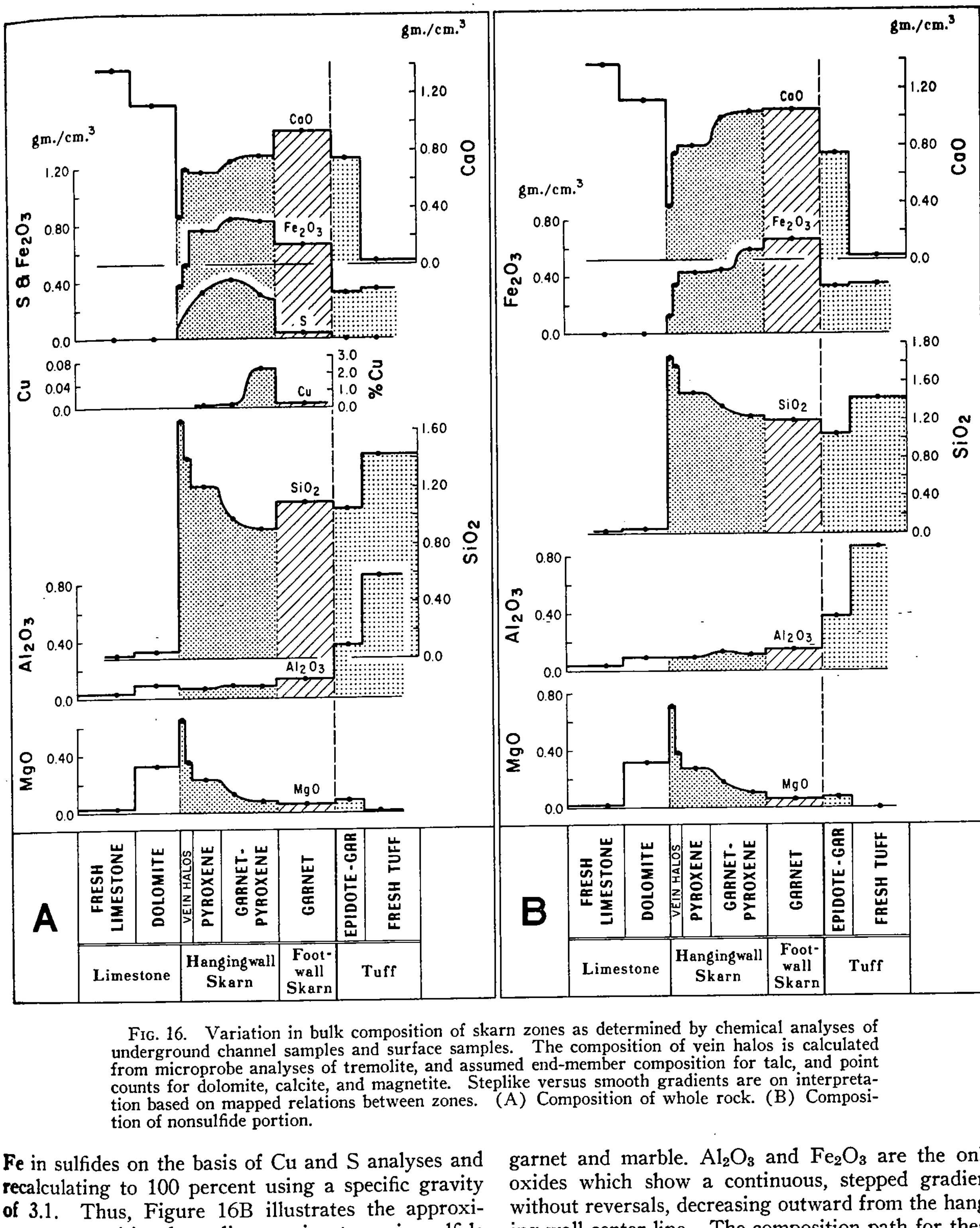

FIG. 16. Variation in bulk composition of skarn zones as determined by chemical analyses of underground channel samples and surface samples. The composition of vein halos is calculated from microprobe analyses of tremolite, and assumed end-member composition for talc, and point counts for dolomite, calcite, and magnetite. Steplike versus smooth gradients are on interpretation based on mapped relations between zones. (A) Composition of whole rock. (B) Composition of nonsulfide portion.

Fe in sulfides on the basis of Cu and S analyses and recalculating to 100 percent using a specific gravity of 3.1. Thus, Figure 16B illustrates the approximate compositional gradients prior to main sulfide deposition.

The most interesting aspect of the bulk chemistry is the significant divergence of the composition path from a simple gradation in composition between garnet and marble. Al_2O_3 and Fe_2O_3 are the only oxides which show a continuous, stepped gradient without reversals, decreasing outward from the hanging-wall center line. The composition path for these two oxides approximates the gradation in composition between garnet and marble. All other oxides display either culminations (SiO_2, MgO) or depressions (CaO), and CaO and SiO_2 both exhibit gradients which are opposite to a gradation in composition between garnet and marble. Such culminations or depressions with respect to certain components are a common feature of metasomatic rocks and have been discussed in theoretical terms by J. B. Thompson (1959), Korzhinskii (1970), and A. B. Thompson (1975a). In multicomponent systems the bulk composition of any point in a metasomatic column will in general not lie on a simple compositional axis defined by the end members of the column. This is a consequence of the fact that an arbitrary chemical potential gradient may lead to saturation with a phase which contains a greater amount of a certain component than phases on either side. Such a process may be visualized with the help of Figure 12, where an increase in μ_{Si} and a decreased in μ_{Mg} toward the vein centers was proposed in a previous section to account for the zonal sequence DoCc-TaCc-Ta-Tr(Cc)-DiCc on the marble contact. In this example, the composition gradients for SiO_2 and MgO show a depression in the Ta zone, whereas CaO shows a culmination in the Ta zone. This suggests that transport of a given component can occur up its own concentration or chemical potential gradient ("uphill diffusion," Cooper, 1974).

Summary and Conclusions

Skarn formation at the MVM resulted in the development of an early garnet zone consisting predominantly of grandite (Ad_{30-70}) and lesser pyroxene (Hd_{0-25}). Garnet/garnet + pyroxene fractions show no systematic variation from an average value of 0.8. Dolomitization of marble may have occurred during this stage, but the contact between marble and garnet is obscured by the later development of the main sulfide-bearing portion of the skarn.

The later, sulfide-bearing portion is characterized by the zonal pattern: Do, TaMt, Tr, SaMtHmPy, GrSaPy. Calcite is present throughout and is interpreted as being contemporaneous with silicates. The sequence of mineral formation in individual samples is in general the same as their zonal sequence toward the skarn center. The iron content of pyroxene passes through a maximum in pyroxene vein centers on the marble contact and then gradually diminishes toward the skarn center. Pyroxene contemporaneous with grandite is less iron rich than earlier pyroxene formed at the same point in the pattern. As the iron content of grandite exceeded Ad_{80}, pyroxene deposition ceased, and chalcopyrite deposition commenced with the replacement of pyroxene by Ad_{100}. As these late ore fluids encroached on successively more iron rich pyroxenes beyond the pyroxene-garnet zone, pyroxene was replaced by actinolite.

Textures and mineral compositions clearly indicate that the process of skarn formation involved only local equilibrium between fluid and wall rocks. Large variations in composition of phases within grains and between adjacent assemblages preserve the record of skarn growth. Reconstitution of early assemblages by later fluids in the garnet-pyroxene zone was restricted to the immediate vein walls, and the majority of late silicates appear to have been deposited in open spaces. The apparent gradual decrease in garnet/garnet + pyroxene from 0.75 to 0.00 toward marble for the deposit as a whole reflects the varying degree of replacement and vein filling by a series of assemblages which actually display fairly abrupt changes in proportions of phases.

The MVM zonal pattern may be interpreted in terms of a contemporaneous zonal growth model in which the zone mineralogy and phase composition were controlled both by gradients in the chemical potentials of nonvolatile components and by changes in T-X_{CO_2}. In general, however, the skarn assemblages are of too high a variance to allow the conclusive separation of chemical and physical variables. Petrogenetic interpretations are further hampered by the lack of experimental data on the effect of iron on the Mg end member reactions.

Comparison of the MVM skarn with published accounts of other skarns yields the following points which may serve to outline areas for further study:

(1) The zonal pattern at the MVM resembles in a general way sequences described from Hanover, Central mining district, N. M. (Schmitt, 1935), Linchburg mine, Magdalena district, N. M. (Titley, 1961), San Antonio mine, Santa Eulalia district, Mexico (Hewitt, 1943), Prescott mine, Texada Island, B. C. (Swanson, 1925), Yaguki mine, Japan (Shimazaki, 1969), Shinyama mine, Japan (Tsusue, 1961), and Kurusay, U.S.S.R. (Tarasov, 1966). These sequences have been generalized by Burt (1974) into four zones: (1) vein, intrusive, or magnetite zone, (2) andraditic garnet zone, (3) hedenbergite zone, and (4) marble zone. This pattern is distinct from other calcium skarns which develop a wollastonite zone between pyroxene and nondolomitic marble and from magnesium skarns which are characterized by forsterite, serpentine, and magnetite. The presence of TaMtCc assemblages, such as those at the MVM, is not documented in the above occurrences, although an equivalent assemblage with chlorite instead of talc occurs with hematite on the marble contact at Linchburg (Titley, 1961).

(2) The majority of the above references do not contain information on the composition trends of phases within the zonal sequence. One exception is the study of the Second Copper orebody at the

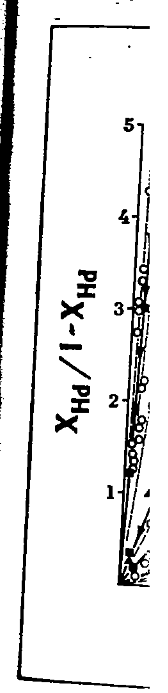

Shinyama mine, where Tsusue (1961) has documented a sequence very similar to that at the MVM: a dark-green pyroxene (Hd_{80}) zone separates marble from a garnet-pyroxene zone which contains $Ad_{40}Hd_{50-65}$. Late Ad_{95} veins cut the garnet-pyroxene zone. The paragenetic trends in garnet composition at the Razdan magnetite-bearing skarn, Soviet Armenia (Bojadzan, 1969), are also similar to those at the MVM; early fragments of Ad_{30-74} + pyroxene are cemented by Ad_{70-85} + magnetite, and both early garnet generations are cut by local veinlets of Ad_{88-97}. The majority of studies of zonal composition trends deal with tungsten-bearing skarns: Fujigatani mine, Japan (Ito, 1962), Strawberry mine, California (Nokleberg, 1970), and Pine Creek, California (Wright, 1973). In contrast with copper-bearing skarns, such as the MVM and Shinyama, these tungsten skarns contain relatively iron poor grandites and relatively iron rich pyroxenes, and the iron content in both of these phases *decreases* toward marble. Similar tungsten-bearing skarns of the Mount Morrison pendant, Sierra Nevada, have been studied by Morgan (1975) with the general conclusion that early magnesian pyroxene is followed by grandite coexisting with a more iron rich pyroxene.

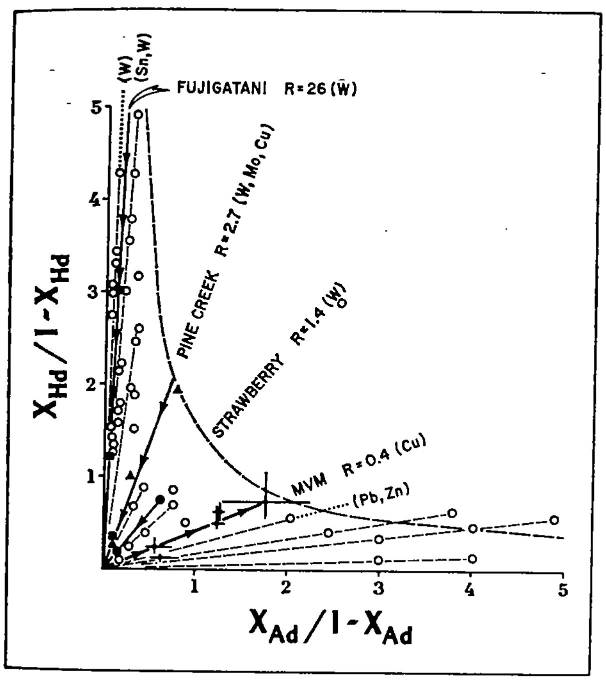

FIG. 17. The compositions of coexisting garnets and pyroxenes in skarns expressed as $X_{Hd}/1\text{-}X_{Hd}$ versus $X_{Ad}/1\text{-}X_{Ad}$. Open circles are from Zharikov (1970, fig. 122). Thin dashed lines join data points from individual deposits. Black symbols indicate additional data from North American and Japanese skarns referred to in text. The zonal position of each black datum point within a given skarn is indicated by the solid lines with arrows pointing toward marble. The curved, dashed line represents $X_{Ad} + X_{Hd} = 1.1$. $R = (X_{Hd}/1\text{-}X_{Hd})/(X_{Ad}/1\text{-}X_{Ad})$.

TABLE 7. Coexisting Garnet-Pyroxene Pairs, from the Footwall (FW) and Hanging-Wall (HW) Skarns

	Garnet		Pyroxene			
Sample	Grain no.	X_{Ad}	Grain no.	X_{Hd}	$X_{Hd} + X_{Ad}$	R
FW 4-4	2A	0.36	3B	0.20	0.56	0.44
FW 3-6	1A (core)	0.38	1C	0.10	0.48	0.19
HW 4-3A	1A	0.55	1E	0.34	0.89	0.41
HW 3-50	1A	0.56	1D	0.39	0.95	0.50
HW 3-53	2A (core)	0.64	2B	0.43	1.07	0.42

$R = (X_{Hd}/1 = X_{Hd})/(X_{Ad}/1 = X_{Ad})$.

(3) Figure 17 summarizes the available data, largely from Zharikov (1970), on the compositions of coexisting garnets and pyroxenes in skarns. The following are some of the more important features of the diagram:

a) The value of $X_{Ad} + X_{Hd}$ for coexisting garnet-pyroxene pairs is generally less than 1.1 for most skarns (Table 7). Thus, coexisting garnets and pyroxenes tend to exhibit a mutual increase or mutual decrease in iron content, but relatively high iron content in both phases is generally excluded due to the different oxidation states of iron in the two phases. The coexistence of relatively iron rich garnets and pyroxenes may be possible at high temperature (Burt, 1971), but there are no documented occurrences of coexisting andradite and hedenbergite in skarns.

b) Continuous, systematic variation in garnet and pyroxene compositions is characteristic of the garnet-pyroxene zones of individual skarns. Numerous deposits show three or more data points defining a significant spread in mineral compositions. More data are clearly required on mineral composition variations within zoning sequences, because such data have direct bearing on the application of Korzhinskii's (1970) diffusion versus infiltration models for metasomatic processes.

c) Skarns tend to exhibit constant values of X_{Hd}/X_{Ad} for coexisting garnet-pyroxene pairs. Samples with values of X_{Hd}/X_{Ad} which differ significantly from the majority of other samples in a given skarn may represent a separate silication episode. Evidence supporting this interpretation is supplied by sample 3–6, MVM, which represents the early hornfels stage rather than the main hanging-wall skarn stage (Table 7).

d) Copper-lead-zinc skarns have lower X_{Hd}/X_{Ad} values than tungsten-molybdenite skarns, as first documented by Zharikov (1970). Such a systematic relationship emphasizes the genetic tie between silicate and ore mineralogy and could prove to be an important exploration tool. The ratio X_{Hd}/X_{Ad} may be useful for classifying skarn deposits because it provides an oxidation scale for garnet-pyroxene assemblages. This relationship could also form the basis for defining the chemical and physical environments of transport and deposition of copper versus tungsten.

Acknowledgments

The present paper is a portion of a continuing geological study of the Yerington district by the geology staff of the The Anaconda Company. The writer is particularly indebted to John M. Proffett, Jr., for his help during the initial phases of the investigation. His definition of the district stratigraphic and structural setting was invaluable. Grateful acknowledgment is also made to John P. Hunt, Lewis B. Gustafson, and Richard C. Baker for their support and encouragement. The rock analyses were made in the analytical laboratory of The Anaconda Company in Salt Lake City, under the supervision of Harold Vincent. D. Severson kindly prepared the illustrations. William P. Nash of the University of Utah aided in the microprobe analyses. An early version of this paper benefitted greatly from the perceptive reviews of D. M. Burt, J. G. Liou, and T. Gerlach.

DEPARTMENTS OF APPLIED EARTH SCIENCES AND GEOLOGY
STANFORD UNIVERSITY
STANFORD, CALIFORNIA 94305
March 5, November 30, 1976

References

Bartholomé, P., and Evrard, P., 1970, On the genesis of the zoned skarn complex at Temperino, Tuscany, *in* Problems of hydrothermal ore deposition: Internat. Union Geol. Sci. [Pub.], ser. A, no. 2, p. 53–57.

Bojadzan, M. T., 1969, Garnet at the Razdan contact metasomatic magnetite ore deposit: Acad. Sci. Armenia, Earth Sci. Ser., Bull., no. 2, p. 51–55.

Burt, D. M., 1971, Some phase equilibria in the system Ca-Fe-Si-C-O: Carnegie Inst. Washington Year Book 70, p. 178–184.

—— 1974, Metasomatic zoning in Ca-Fe-Si exoskarns, *in* Hofmann, A. W., and others, eds., Geochemical transport and kinetics: Carnegie Inst. Washington Pub. 634, p. 287–293.

Cermignani, C., and Anderson, G. M., 1973, Origin of a diopside-tremolite assemblage near Tweed, Ontario: Canadian Jour. Earth Sci., v. 10, p. 84–90.

Cooper, A. R., Jr., 1974, Vector space treatment of multicomponent diffusion, *in* Hofmann A. W., and others, eds., Geochemical transport and kinetics: Carnegie Inst. Washington Pub. 634, p. 15–30.

Gordon, T. M., and Greenwood, H. J., 1970, The reaction: dolomite + quartz + water = talc + calcite + carbon dioxide: Am. Jour. Sci., v. 268, p. 225–242.

Greenwood, H. J., 1967, Wollastonite: stability in H_2O-CO_2 mixtures and occurrence in a contact metamorphic aureole near Salmo, British Columbia, Canada: Am. Mineralogist, v. 52, p. 1669–1680.

Hewitt, W. P., 1943, Geology and mineralization of the San Antonio mine, Santa Eulalia district, Chihuahua, Mexico: Geol. Soc. America Bull., v. 54, p. 173–204.

Ito, K., 1962, Zoned skarn of the Fujigatani mine, Yamaguchi prefecture: Japanese Jour. Geology Geography, v. 33, p. 169–190.

James, L. P., 1976, Zoned alteration in limestone at porphyry copper deposits, Ely, Nevada: ECON. GEOL., v. 71, p. 488–512.

Kerrick, D. M., 1974, Review of metamorphic mixed volatile (H_2O-CO_2) equilibria: Am. Mineralogist, v. 59, p. 729–762.

Knopf, A., 1918, Geology and ore deposits of the Yerington district, Nevada: U. S. Geol. Survey Prof. Paper 114, 68 p.

Korzhinskii, D. S., 1959, Physicochemical basis of the analysis of the paragenesis of minerals: New York, Consultants Bur., Inc., 142 p.

—— 1970, Theory of metasomatic zoning: Oxford, Clarendon Press, 162 p.

Meyer, C., and Hemley, J. J., 1967, Wall rock alteration, *in* Barnes, H. L., ed., Geochemistry of hydrothermal ore deposits: New York, Holt, Rinehart and Winston, p. 166–235.

Morgan, B. A., 1975, Mineralogy and origin of skarns in the Mount Morrison pendant, Sierra Nevada, California: Am. Jour. Sci., v. 275, p. 119–142.

Mueller, R. F., 1961, Analysis of relations among Mg, Fe, and Mn in certain metamorphic minerals: Geochim. et Cosmochim. Acta, v. 25, p. 267–296.

Noble, D. C., 1962, Mesozoic geology of the southern Pine Nut Range, Douglas County, Nevada: Unpub. Ph.D. thesis, Stanford University, 200 p.

Nokleberg, W. J., 1970, Geology of the Strawberry mine roof pendant, central Sierra Nevada, California: Unpub. Ph.D. thesis, University of California, Santa Barbara, 157 p.

Proffett, J. M., Jr., 1969, Report on the geology of the Yerington district: Unpub. company rept., The Anaconda Co., 404 p.

—— 1972, Nature, age, and origin of Cenozoic faulting and volcanism in the Basin and Range Province (with special reference to the Yerington district, Nevada): Unpub. Ph.D. thesis, University of California, Berkeley, 77 p.

Proffett, J. M., Jr., and Proffett, Beth, 1976, Stratigraphy of the Tertiary ash flow tuffs in the Yerington district, Nevada: Nevada Bur. Mines Geology Rept. 27, 28 p.

Schmitt, H., 1935, The Central mining district, New Mexico: AIME Trans., v. 115, p. 187–208.

Shimazaki, H., 1969, Pyrometasomatic copper and iron deposits of the Yaguki mine, Fukushima prefecture, Japan: Univ. Tokyo Fac. Sci. Jour., sec. 2, v. 17, p. 317–350.

Skippen, G. B., 1967, An experimental study of metamorphism of siliceous carbonate rocks: Unpub. Ph.D. thesis, Johns Hopkins University, 251 p.

—— 1971, Experimental data for reactions in siliceous marbles: Jour. Geology, v. 79, p. 457–481.

—— 1974, An experimental model for low pressure metamorphism of siliceous dolomitic marble: Am. Jour. Sci., v. 274, p. 487–509.

Slaughter, J., Kerrick, D. M., and Wall, V. J., 1975, Experimental and thermodynamic study of equilibria in the system CaO-MgO-SiO_2-H_2O-CO_2: Am. Jour. Sci., v. 275, p. 143–162.

Swanson, C. O., 1925, The genesis of the Texada Island magnetite deposits: Canada Geol. Survey Summary Rept., pt. A, p. 106–144.

Tarasov, V. A., 1966, On the formation of skarn-polymetallic deposits at Kurusay: Geochemistry Internat., v. 3, p. 628–635.

Taylor, B. E., and Liou, J. G., 1975, Low-temperature stability of andradite in C-O-H fluids; experimental and field data: Am. Geophys. Union Trans., v. 56, p. 1071.

Thompson, A. B., 1975a, Calc-silicate diffusion zones between marble and pelitic schist: Jour. Petrology, v. 16, p. 314–346.

—— 1975b, Mineral reactions in a calc-mica schist from Gassets, Vermont, U. S. A.: Contr. Mineraology Petrology, v. 53, p. 105–128.

Thompson, J. B., Jr., 1959, Local equilibrium in metasomatic processes, *in* Abelson, P. H., ed., Researches in geochemistry: New York, John Wiley and Sons, p. 427–457.

Titley, S. R., 1961, Genesis and control of the Linchburg orebody, Socorro County, New Mexico: Econ. Geol., v. 56, p. 695–722.

Tsusue, A., 1961, Contact metasomatic iron and copper ore deposits of the Kamaishi mining district, northeastern Japan: Univ. Tokyo Fac. Sci. Jour., sec. 2, v. 13, p. 133–179.

Vidale, R. J., and Hewitt, D. A., 1973, "Mobile" components in the formation of calc-silicate bands: Am. Mineralogist, v. 58, p. 991–997.

Wright, W. A., 1973, Skarn formation at Pine Creek mine, Bishop, California: Unpub. Ph.D. thesis, University of California, Berkeley, 135 p.

Zharikov, V. A., 1970, Skarns: Internat. Geology Rev., v. 12, p. 541–559, 619–647, 760–775.

wed by moderate
erminated by the
posits associated
ce swarms within
monzonite por-
)atholith in vary-
und south of the
of Triassic sedi-

ussion of contact
of Triassic rocks
esented elsewhere.
re to set the con-
tribution of meta-
neral assemblages
h, rather than the
for these effects.
odes, as first docu-
ly stage produced
the batholith con-
rnblende hornfels
n the metasomatic
te-andradite series
ent andradite. The
edenbergite series
o 15 mole percent

elses was followed
arnets without py-
ik clinozoisite near
tion of andradite-
ietasomatic aureole
leposits are located
on. Two of these,
eposits, are located
contact within the
rnfelses. Both are
low total sulfides,
ent; (2) relatively
generally greater
e or hematite; (4)
e, with minor epi-
strong brecciation.
the andradite-chal-
ig four producers:
, Casting Copper,
order of decreasing
dolomitized marble
lses, 1,000 to 2,000
These fringe skarns
vely high total sul-
lume percent; (2)
os, generally lower
intities of magnetite
ngue dominated by
te; (5) little or no

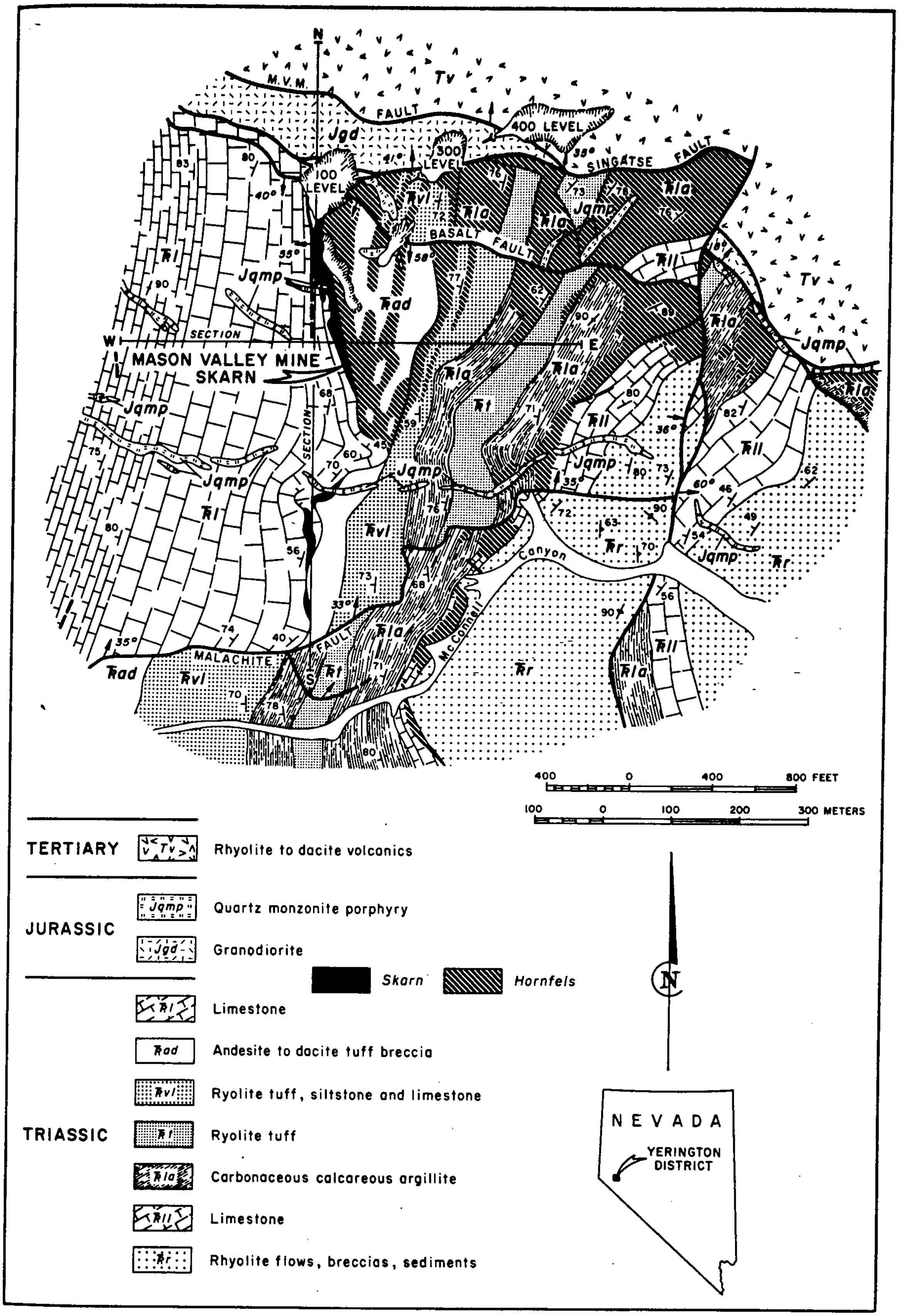

FIG. 1. Surface geologic map of the vicinity of the Mason Valley mine. Irregularity of flat fault traces is due to topography. Insert shows location of Yerington district in western Nevada.